High resolution, large area vision-based tactile sensing based on a novel piezoluminescent skin

Ruxiang Jiang, Lanhui Fu, Yanan Li, *Senior Member, IEEE*, and Hareesh Godaba

***Abstract*—The ability to precisely perceive external physical interactions would enable robots to interact effectively with the environment and humans. While vision-based tactile sensing has improved robotic grippers, it is challenging to realize high resolution vision-based tactile sensing in robot arms due to presence of curved surfaces, difficulty in uniform illumination, and large distance of sensing area from the cameras. In this paper, we propose a novel piezoluminescent skin that transduces external applied pressures into changes in light intensity on the other side for viewing by a camera for pressure estimation. By engineering elastomer layers with specific optical properties and integrating a flexible electroluminescent panel as a light source, we develop a compact tactile sensing layer that resolves the layout issues in curved surfaces. We achieved multipoint pressure estimation over an expansive area of 502 sq. cm with high spatial resolution, a Two-Point Discrimination distance of 3 mm horizontally and 5 mm vertically which is comparable to that of human fingers as well as a high localization accuracy (RMSE of 1.92 mm). These promising attributes make this tactile sensing technique suitable for use in robot arms and other applications requiring high resolution tactile information over a large area.**

***Index Terms*—Vision-based sensing, tactile sensor, Two-Point Discrimination, pressure estimation**

I. Introduction

TACTILE receptors serve as the foundation for human engagement with the environment. Because of the abundant tactile receptors, humans are able to gather information about the properties of objects in our environment enabling us to interact with them and execute intricate and precise movements [1]. With the growing range of applications for robots, it is crucial to improve their versatility in physically interacting with the environment as well as humans. For this purpose, it is imperative to develop the capability of robots to obtain tactile information from diverse geometries, including the links and other relevant parts [2]. Furthermore, tactile sensors should be conformable to the range of geometries in the target applications while being robust [3].

Significant efforts have been put into developing different tactile sensing technologies to achieve large area capabilities using both discrete and continuous methods. Electrical tactile sensing skins are typically designed with a densely arranged array of sensing units and can be broadly categorized based on their operational principles as capacitive, resistive, inductive, or optical-based sensors [4]. Tactile sensors based on rigid materials such as capacitive touch sensing found in common mobile phone touchscreens, are limited to providing positional information upon touch [5]. Soft electrical tactile sensors capable of localizing touch and estimating the magnitude of pressure typically necessitate complex circuitry and signal processing to handle large streams of data from all the individual sensing receptors [6]. Their resolution is constrained by the density and layout of the sensing receptors, for example, the layout of electrodes in a capacitive sensing skin [7]. Furthermore, they also demand intricate customized designs to cater to different surface geometries [8]. Vision-based tactile sensing methods exploit the ability of the camera to observe a large area with high resolution and leverage image processing and computational techniques to convert deformation cues in images into tactile sensing information [9]. Due to their utilization of optical design and optical signals for discerning tactile signals, vision-based tactile sensors exhibit superior resistance to electromagnetic interference. Consequently, their output signals are comparatively more stable and reliable in a range of environments [10]. The ability of vision-based sensors to achieve high resolution tactile information has helped them rapidly gain attention in the field of tactile sensing.

Soft elastomers such as Ecoflex 00-30 or Polydimethylsiloxane (PDMS) are employed as a medium for transducing force or pressure signals into visually detectable information and cameras are used to capture real-time images that can be related to tactile information [11]. The majority of vision-based tactile sensing methods involve reflective membranes or tracking displacement of markers, as exemplified by GelSight and TacLINK sensors [12]–[14]. Employing very soft materials such as gels to enhance sensitivity results in large hysteresis affecting the bandwidth of the sensors. Reflective membranes illuminated with different colors have also been utilized for estimating normal forces in a small region such as a sensor fingertip and for texture detection in a large cylindrical roller [12], [15]. For large-area tactile sensing systems, using a reflective membrane approach may involve more complex optical design and require precise positioning of light sources. While this method is effective for texture detection, its design may pose challenges for accurately assessing normal forces over large cylindrical surfaces, due to potential limitations in ensuring consistent light reflection back to the camera from all parts of the tactile sensing surface.

To address the aforementioned shortcomings of existing tactile sensing techniques for large area tactile sensing, this paper introduces a novel vision-based tactile sensing approach that transduces applied pressure on a skin into a change in

This work was supported in part by the Sussex Higher Education Innovation Fund, and PhD Research Start-up Fund of Wuyi University (No. BSQD2222).

Ruxiang Jiang and Yanan Li are with the Department of Engineering and Informatics, University of Sussex, Brighton BN1 9RH, UK. Hareesh Godaba is with the Department of Mechanical Engineering, University of Southampton, Southampton SO17 1BJ, UK. Lanhui Fu is with School of Electronics and Information Engineering, Wuyi University, Jiangmen 529020, China. (e-mail:yl557@sussex.ac.uk, h.godaba@soton.ac.uk)

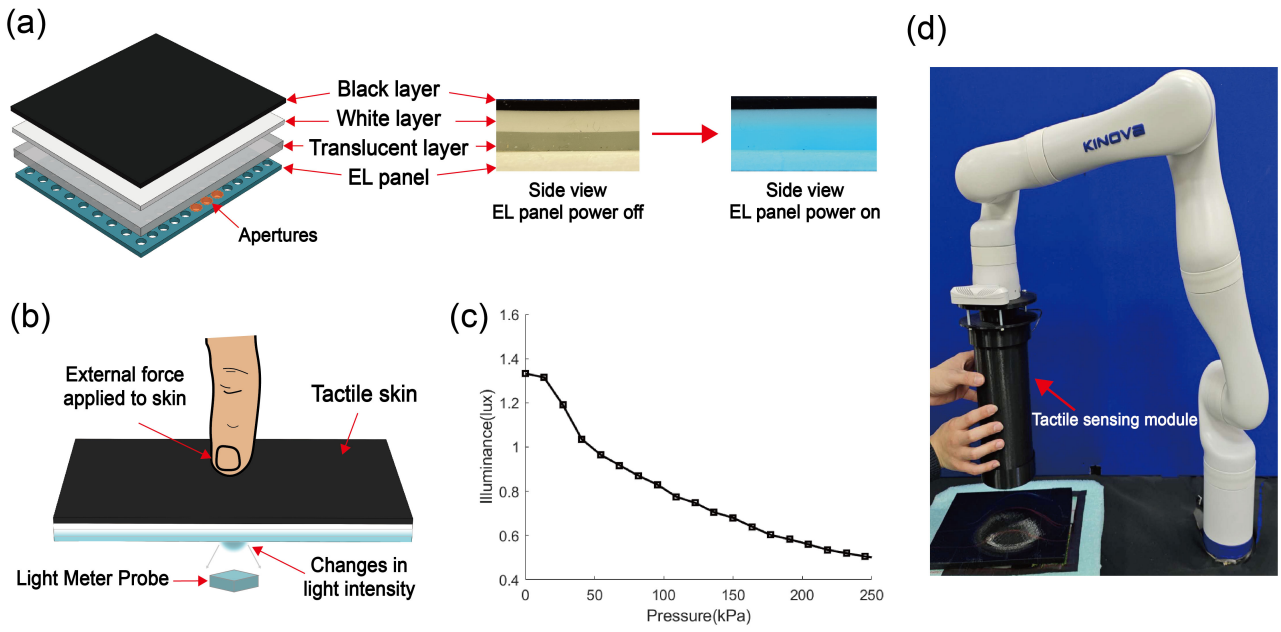

Fig. 1. (a) Illustration of the laminated structure of the piezoluminescent skin along with the images of the side view before and after activating the electroluminescent (EL) panel as captured by a camera. (b) When pressure is applied to a specific area of the piezoluminescent skin, the light intensity emitted through the aperture in that region decreases. (c) Illuminance measured from a single aperture in relation to applied pressure. (d) A tactile sensing module based on the piezoluminescent skin is mounted on a robot arm to enable human guidance of the robot movement.

light intensity at that area. This skin integrates an electroluminescent (EL) panel with apertures as a planar light source and three soft elastomer layers with different optical properties to function as transmitting, reflective, and opaque layers. We refer to the combined four layers as the piezoluminescent skin, which works together to modulate the light intensity emitted based on the applied pressure (Fig. 1(a)). The light from the EL panel undergoes diffuse reflection within the translucent layer and surface reflection from the white layer to result in light emission through the apertures in the EL panel. When pressure is applied on the black opaque layer, the deformation in the elastomer layers causes the light intensity emitted through the apertures to decrease (Fig. 1(b)). The light intensity from the piezoluminescent skin decreases consistently for pressures ranging from 0 to 250 kPa providing a simple transducing mechanism to estimate pressure using light intensity (Fig. 1(c)). Monitoring the light intensity emitted from the apertures of the piezoluminescent skin by using a camera enables the detection of physical contact as well as the estimation of the magnitude of pressure applied at each aperture. Optimizing the multilayer structure of the piezoluminescent skin, we realized a cylindrical tactile sensor capable of achieving multi-point touch detection and pressure estimation over a large area. The cylindrical tactile sensor can be utilized as a sub-end effector providing an interface for physical human-robot interaction (pHRI) to enable intuitive human guidance for robot manipulators (Fig. 1(d)).

The rest of the paper is organized as follows. Section II describes related works. Section III introduces the working principle of the piezoluminescent skin and Section IV discusses the optimization of various design parameters of the piezoluminescent skin to improve its sensitivity to pressure. Section V describes the design of the large area cylindrical and fabrication technique. Section VI describes the camera calibration model and the method employed for pressure calibration. Section VII discusses the performance evaluation of the sensor and demonstrates the multi-point contact localization and pressure estimation capabilities of the sensor. Section VIII conducts a comparative analysis with other relevant works and outlines the key limitations of the proposed sensor. Finally, Section IX describes the conclusions and outlines future work.

II. Related Works

Tactile sensors have a wide range of applications in the field of robotics. In comparison to conventional force sensors, tactile sensors offer multimodal perceptual information, encompassing parameters such as contact area, pressure distribution, slip detection, and surface characteristics of objects. This information plays a crucial role in facilitating the interaction of robots with objects, the environment and also ensuring the safety of interactions between humans and robots [16], [17].

The importance of tactile sensing in robotics is underlined by the extensive applications witnessed in the literature. Large-area tactile sensing systems, where the robot is embedded with sensing abilities over an extended region, have prominently featured in applications involving humans in order to allow versatility in the range of interactions humans can make with the robots [18]–[20]. We now discuss the salient vision-based and electronic-based sensing methodologies for achieving large-area tactile sensing.

A. Vision-based Tactile Sensors

Johnson et al. first introduced a vision-based method for the measurement of shape and texture utilizing elastomeric materials to transduce deformation into visible optical patterns [21]. This approach demonstrated the effectiveness of combining the high resolution offered by cameras and the compliance of soft elastomers in enabling the detection of rich contact information. Yuan et al. developed GelSight tactile sensors capable of estimating shear force and detecting slip for use in grippers. By illuminating the sensor's contact surface with three different colors of light (RGB) and analyzing the reflections of these colors using a camera, accurate detection of the surface shape of the object and subsequently estimation of force distribution were realized [22]. Similarly, Lin et al. developed DTact, which employs the reflective properties of a multilayered semi-transparent elastomer to effectively estimate the 3D geometry of a contact object from darkness in captured images [23]. Li et al. developed a tactile sensor specifically for global normal force and moment estimation along with detailed tactile information [24]. The sensor utilized an elastomer with added reflective powder and an LED array as the light source. When a force is applied, the contact area between the reflective elastomer and the acrylic plate increases. By capturing the light intensity with a camera, the magnitude of the normal force could be estimated. Ward-Cherrier et al. introduced the TacTip family of sensors, which encompasses various structural designs with distinct applications and performance characteristics [25].

Many of the methods used for sensing in small regions are challenging to extend for large area sensing. For example, methods based on the reflection of monochromatic or polychromatic light and diffraction patterns require complex illumination system design to allow homogeneous illumination of curved surfaces as well as to prevent artifacts in camera images due to unintended internal reflections.

For large area tactile sensing based on vision, studies mainly focused on tracking marker movement due to external forces. Cao et al. proposed Touchroller, a cylinder-shaped tactile sensor with a roller structure, which exhibits high accuracy in collecting texture information [15]. When the sensor rolls on the surface of an object, a camera captures a series of continuous images, enabling the effective reconstruction of large surface textures. However, this technique has only a limited viewing area at a given time and is not aimed at force estimation. Zhang et al. introduced a cylinder-shaped tactile sensor based on tracking markers on a transparent elastomer layer attached to a transparent cylindrical tube [26]. This sensor was utilized as an effective link of a robot and experiments for human contact motion following were conducted demonstrating intuitive interaction with humans. While contact detection was demonstrated, it is challenging to achieve accurate force estimation using this technique due to the limited displacement of markers on a thin elastomer layer and the challenge associated with the reduced footprint of regions far from the camera. Winstone et al. proposed a remote tactile sensing capsule endoscopy system that utilizes a design similar to Tactip, capable of discriminating the shape, size, and softness of bowel deformities. In this design, the tactile sensor relies on large displacements of markers on the skin to map force signals, resulting in a relatively large Two-point Discrimination (TPD) distance. Additionally, since the camera is positioned at the base of the structure, markers that are farther away from the camera exhibit smaller displacements in the images, which limits the system's detection area and sensitivity [27]. Duong et al. developed a large-scale vision-based tactile sensor based on tracking markers on the inside surface of a pressurized silicone structure [14]. At low internal air pressures, the marker displacement is highly sensitive to the applied force allowing accurate estimation of applied force. However, this heightened sensitivity imposes limitations on its load-bearing capacity, necessitating a delicate balance in air pressure adjustments. Fu et al. recently introduced a large area cylindrical tactile sensing module called ELTac that employs flexible EL panels integrated with deformable elastomeric pyramids that modulate the light intensity from the EL panels based on applied pressure [28]. However, due to EL panels being set at the outermost layer of the skin and the inherent hardness of the EL panel itself, the pressure applied in a confined area will transmit to the surrounding area, limiting its ability to distinguish multiple close contact regions. Additionally, the pyramidal arrays needed for the skin make it challenging to achieve monolithic sensor skin reducing the coverage and introducing inhomogeneities at the borders of sensor units.

B. Electronic-based Large Area Tactile Sensors

For large area electronic-based tactile sensors, Schmitz et al. proposed ROBOSKIN, a modular tactile sensor in which modular units can be simply added or removed. They employed a flexible PCB board to meet the requirements for curved surface applications. Moreover, through I^2C serial communication, information from multiple sensor modules could be monitored with a single microcontroller. The ROBOSKIN sensing system could be integrated into a variety of existing robot hardware with a low degree of customization [29]. While the sensing range is large in the order of 100 kPa, the small dimension of each sensing unit results in a pressure resolution of around 1 kPa making it challenging to further increase taxel density. Furthermore, as the number of sensor modules increases, the system may encounter complex wiring and readout latency. Lee et al. introduced the Asynchronously Coded Electronic Skin (ACES), a signal transmission scheme inspired by the functionality of biological nerves. It can transmit information simultaneously in an event-based sensing system with even more than 10000 sensors. A tactile sensing system with 240 sensing units and a time latency of 1 ms for event detection was demonstrated [30]. To simplify the circuit system of tactile skins and enhance their scalability and stretchability, the Electrical Resistance Tomography (ERT) method to detect forces on a soft conductive sheet was introduced [31], [32].

The placement of electrodes only at the edges of the conductive sheet compromises spatial resolution in the central region of the skin. To optimize the spatial resolution in the central part of the sensing area, Lee et al. introduced dispersed

electrodes throughout the middle section of the entire sensing skin. However, an increase in the number of electrodes leads to a more complex and expensive circuit, imposing limitations on data collection and increasing computational complexity [33], [34]. To address this issue, Lowther et al. introduced the Salt-E-Skin, a fluidic electronic skin that utilizes a network of saline-filled channels to enable conduction detection and Electrical Impedance Tomography (EIT) to localize skin deformation. Although the localization error in the experimental results was relatively high due to a low number of electrodes employed, the work offers insights into how the channel structure can improve this [35].

In summary, the utilization of electronic components as sensing elements presents specific challenges when applied to large area tactile sensing. Sensors with discrete or modular units are difficult to use in covering curved surfaces given the need for rigid electronic components for data readout. When a large area and high-resolution implementation are required, constraints arising from the distribution density sensing units can lead to wiring and manufacturing complexities. Increasing the spatial resolution of tactile sensing through miniaturization of individual electronic sensing elements also leads to a decrease in the base value of the measurand which results in low sensitivity and increase in cost of readout electronics. ERT-based tactile sensors necessitate extensive pre-calibration of data points. Implementation of ERT sensing demands a high sampling rate for the data acquisition unit and high-performance data processing equipment, thereby resulting in high costs and complexity in the implementation of this method in large area applications. In contrast to vision-based sensors, electronic sensors do not require hollow structures that facilitate a direct line of sight from the camera to the sensing surface and can be applied to existing robotic hardware more easily.

Overall, the key challenges in large area tactile sensing include achieving high force sensitivity, accurate pressure estimation robust to loading conditions, the ability to discriminate multiple close contact points, and employing fabrication techniques to ensure optimal coverage with homogeneous sensor characteristics across the sensor area.

III. Working principle of the piezoluminescent skin

To address the overarching challenges in large area tactile sensing, we propose a novel piezoluminescent skin that converts applied pressure to change in light intensity emitted directly at that point as well as provides a soft interface for physical interaction.

The piezoluminescent skin comprises a total of four layers as shown in Fig. 1(a). The innermost or the bottom layer is an electroluminescent panel (EL Panel and Tape, Rhizomic Electronics Ltd), utilized in this sensor system as a planar light source. It is opaque, thin, and flexible allowing the skin to be compliant and can be cut without loss of functionality. We make several apertures in the opaque EL panel using a CNC milling machine to allow the transmission of light through them. The second layer is composed of a translucent elastomer, in which the light emitted from the EL panel undergoes diffused reflection. The third layer is a white opaque elastomer, referred to as the reflective layer, designed to reflect light incident on it from the second layer to enhance light intensity in the translucent layer. The outermost or the top layer is a black opaque elastomer serving to obstruct environmental light from affecting the sensor.

The circular apertures in the EL panel allow the diffused light within the translucent layer to scatter beneath the EL panel which can be captured by a camera. As depicted in Fig. 2(a), before the application of pressure, light entering the translucent layer undergoes reflection from the white reflective layer, with some light scattering out from the apertures in the EL panel. When pressure is applied, the deformation in the reflective layer causes changes in the angle of incidence of light on the reflective layer. Consequently, the light emanating from the apertures in the EL panel diminishes in the region where pressure is applied (Fig. 2(b)). Additionally, due to the reduction in thickness in the translucent layer, the amount of diffused light in this region also decreases. As a result, the light intensity in the contact region decreases in the images captured by the camera with increasing pressure (Fig. 2(b)). This change in light intensity with applied pressure is the main transduction mechanism for sensing based on our proposed piezoluminescent skin.

Employing a camera, the changes in the brightness of light emitted from a specific aperture can be calibrated against known applied pressures. As the viewing angle and the distance from the camera are different for different points on the sensor surface, it is essential to first identify the location of the applied pressure before utilizing the calibration to estimate the pressure applied. Utilizing image-processing techniques and the knowledge of the geometry of the sensing surface, one can obtain the pixel coordinates of the compressed region in the camera image, convert two-dimensional pixel coordinates to three-dimensional positions, and estimate the applied pressure. In contrast to vision-based large area tactile sensors in the literature that require tracking of markers using binocular cameras and estimating the deformation and pressure, our proposed technique directly offers a brightness change at the point of application of pressure on the sensor surface making localization as well as calibration easy. In addition, this technique based on piezoluminescent skin requires only a single camera and also allows detection and estimation of pressure at points far away from the camera. The straightforward construction of the multi-layered skin structure, coupled with the direct correspondence between brightness and pressure applied at the point enables the dense spatial distribution of taxels resulting in high spatial resolution.

IV. Sensor optimization

The sensitivity of the changes in emitted light intensity to applied pressure in the piezoluminescent tactile sensing skin is influenced by various factors such as the geometry and optical properties of the elastomer layers as well as the luminance of the EL panel. These factors are directly related to the phenomenon of light diffusion within the translucent layer.

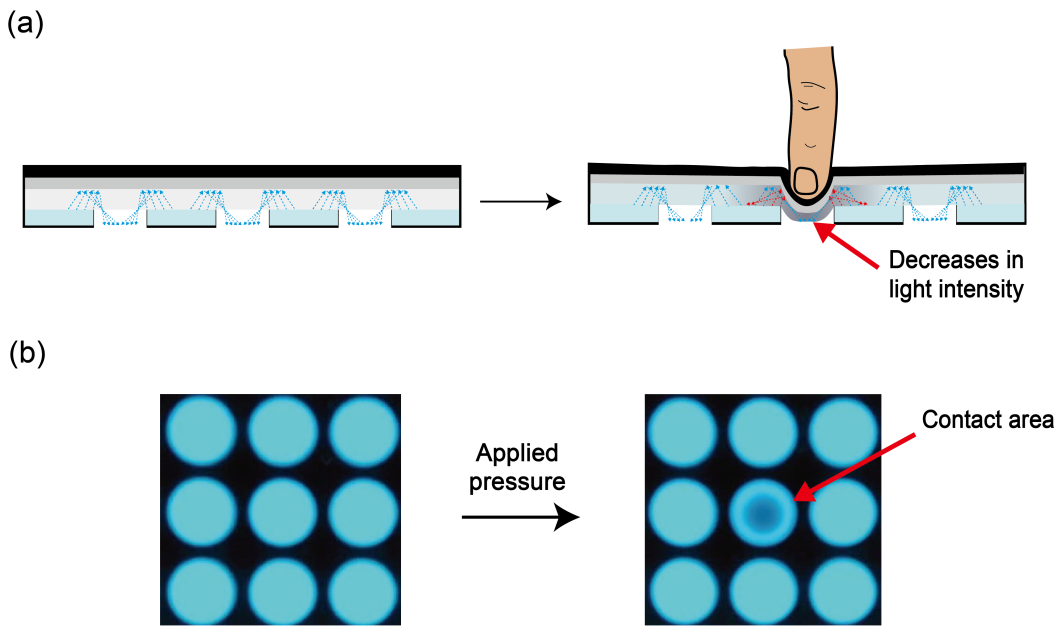

Fig. 2. Principle of operation of piezoluminescent skin (a) Light from the EL panel enters the translucent layer and is reflected by the white reflective layer. When pressure is applied, deformation in the skin changes the angles of incidence reducing the amount of light emitted through the aperture. (b) Images of the apertures before and after the application of pressure. The central taxel becomes darker when pressure is applied to it.

To develop a sensor with high sensitivity, we investigated the influence of the following four controllable parameters- the thickness of the translucent layer, the pigment concentration of the translucent layer, the diameter of apertures in the EL panel, and the operating voltage of the EL panel (Fig. 3(a)).

Fig. 3(b) shows the planar experimental setup used for optimizing the influence of these parameters on the sensor sensitivity. A hollow cuboidal platform from black opaque PLA was 3D printed. The top face of the cuboidal structure houses a transparent acrylic sheet upon which the different designs of piezoluminescent skin can be placed. For these experiments, flat piezoluminescent skins utilizing EL panels of dimensions 110 mm $\times$ 70 mm were fabricated. Each piezoluminescent skin is composed of a 300 μm thick EL panel with an aperture of diameter 4 mm. Above the EL panel is a three-layered elastomer structure made of Smooth-On Ecoflex 00-30 with different optical properties. The first is a translucent layer of a thickness 1, 2 or 3 mm and varying concentrations of white pigment (Silc Pig, Smooth-On, Inc.) to control its transmittance. The second is a reflective white layer of 1 mm thickness and the third or the topmost layer is a 1 mm thick black opaque layer.

Below the acrylic sheet is affixed a light meter, or a USB camera to record changes in light intensity from the taxel when pressure is applied on the piezoluminescent skin. An indenter attached to a force sensor (DBBSMM miniature S-Beam load cell) is mounted on a lead screw driven by a stepper motor to apply and measure pressure on the piezoluminescent skin. A rigid 3D-printed indenter with a square cross-section and areal dimensions of 6 mm $\times$ 6 mm which can cover the pitch of the taxel is used for applying forces. Illuminance is measured for applied pressures ranging from 0 to 250 kPa in 10 kPa increments. For each skin sample of a specific thickness, measurements are taken three times, and the mean of these measurements is used.

Fig. 3(c) shows the change of light intensity from a single taxel when pressure is applied to it for different thicknesses of the translucent layer. For each of the samples with thicknesses of 1 to 3 mm, the light intensity emitted from the taxel decreases with increasing pressures from 0 to 250 kPa demonstrating a broad range of pressure sensing. The initial luminance before applying any pressure is higher in samples with thicker translucent layers as more light can be diffused and reflected through the aperture in the EL layer. From Fig. 3(d), it can be observed that the sensitivity peaks for all three thicknesses at around 40 kPa. The reason for this is as follows. Initially, there is a small cylindrical air gap between the translucent layer and the rigid acrylic plate formed by the wall of the aperture in the EL panel. As the pressure increases, the contact area between the acrylic plate and the translucent layer increases until 40 kPa when the contact area saturates and the sensitivity of deformation to force decreases resulting in a decrease in sensor sensitivity after this peak. The skin with the 1 mm thick translucent layer exhibits the highest sensitivity peak, but it decreases to the lowest level beyond 45 kPa. The 3 mm thickness has the lowest sensitivity peak but maintains a relatively high sensitivity at pressures ranging from 50 to 250 kPa. In summary, the lower thickness of the translucent layer achieves higher peak sensitivity at lower pressures while larger thicknesses offer better sensitivity for a wide range of pressures while giving lower sensitivity at low pressures. However, the magnitude of light intensity emitted from the taxel is also lower as can be noted from Fig. 3(c). Low light intensity can lead to potential noise issues that affect image

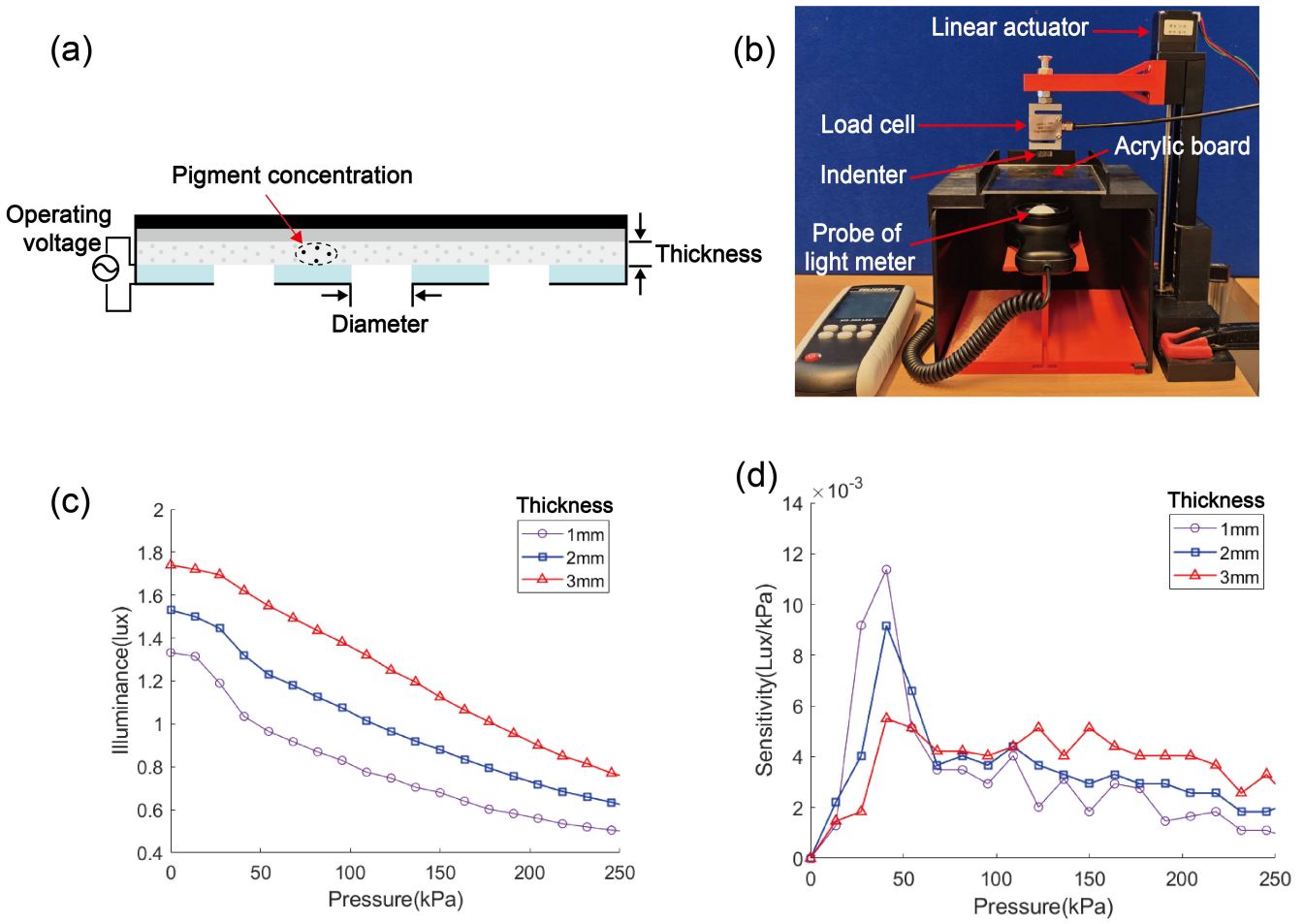

Fig. 3. (a) Design parameters that influence the sensitivity of the tactile sensing skin. (b) Experiment platform for sensor design optimization. (c) Variation in illuminance was measured by the light meter for pressures ranging from 0 to 250 kPa for different thicknesses of the translucent layer. (d) Sensor sensitivity vs pressure for different thicknesses of the translucent layer.

processing. Hence, we choose 2 mm as the thickness for our translucent layer, striking a balance between high sensitivity and adequate light intensity.

In addition to the thickness of the translucent layer, its transmittance as well as the operating voltage of the EL panel affect the light intensity of the emitted light from the taxel. To investigate the effect of transmittance on sensor performance, we added diluted white pigment to the Ecoflex 00-30 pre-cure mixture to reduce transmittance and enhance diffuse reflection within the translucent layer. Initially, 1 g of white pigment was added to 9 g of silicone thinner and mixed thoroughly. Using a micropipette, fixed volumes of the mixture were added to 100 g of Ecoflex 00-30 (A+B mixture) to realize different pigment concentrations. We created three sensing skin samples with three different white pigment concentrations - 0%, 0.01%, and 0.02% by total weight. In this experiment, we utilized a camera mounted inside the experimental platform shown in Fig. 3(b) instead of the light meter. We record an initial image and an image after the application of 20 kPa pressure and convert them to grayscale. The sensitivity is defined as the change of the total grayscale value within the taxel region between the two images divided by the applied pressure of 20 kPa. We observed that an increase in white pigment concentration led to an increase in the initial light intensity. In addition, increasing the operating voltage of the EL panel also led to higher initial light intensity. From Fig. 4(a), we can see that for the same operating voltage, lower pigment density results in increased sensitivity. For a fixed pigment intensity, increasing the voltage improves the sensor sensitivity. Hence, we chose 0% white pigment and set the voltage supplied to the inverter at 12V which corresponds to an inverter output of 100V at 930Hz. It should however be noted that increasing the initial light intensity too much may lead to saturation of grayscale values in the camera images resulting in the reduction of sensor range.

We also fabricated and studied taxels with different diameters mm to identify the influence of taxel diameter on sensor design and performance. We fabricated a piezoluminescent skin by cutting apertures of diameters 2 mm, 4 mm, 6 mm, and 8 mm in an EL panel of dimensions 110 mm $\times$ 70 mm. Using a planar experiment platform and a USB camera, we captured an image of the skin with the EL panel powered on. As the light emitted through the apertures in the EL panel is

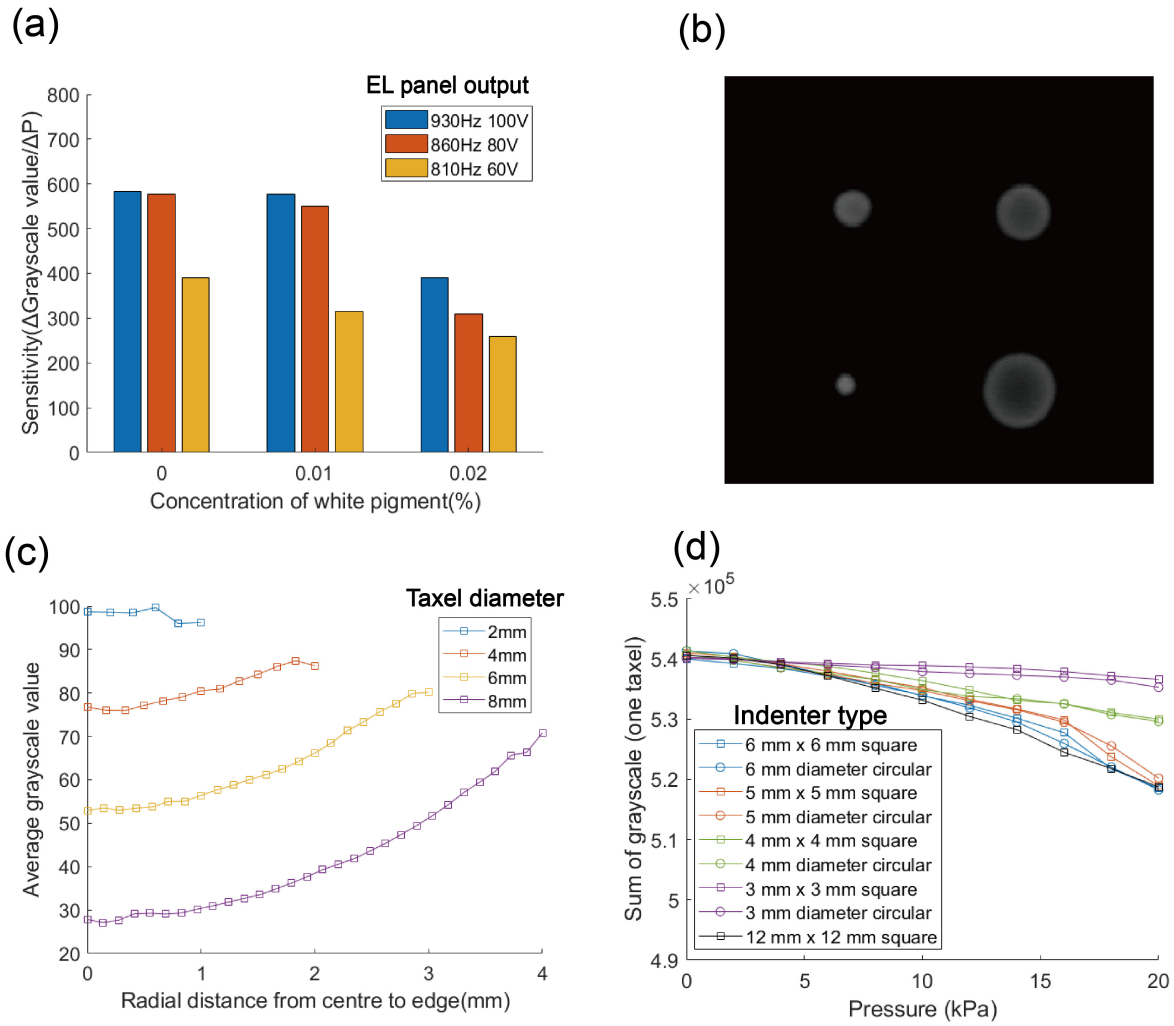

Fig. 4. (a) Influence of operating voltage and pigment concentration of translucent layer on sensor sensitivity. (b) Grayscale image of taxels with different diameters. (c) Variation in average pixel grayscale values with radial distance for taxels of different diameters. (d) Experiment on the pressure response of piezoluminescent skin to indenters of varying sizes and shapes.

from the adjoining area outside the aperture, the light intensity is highest at the boundary of the taxel and reduces towards the center (Fig. 4(b)). We identified the centroid of each taxel and calculated the average grayscale value of the pixels at different radii from the centroid. Fig. 4(c) displays the average grayscale values of pixels at different radial distances from the center to the edge of the circle. When the taxel diameter is greater than 4 mm, the brightness distribution in the taxel becomes uneven, lacking uniformity, and the initial brightness is lower. To obtain a clear and uniformly bright circular emission area in the image we chose a diameter of 4 mm for the taxels.

The shape and size of the indenter are important for calibration of the sensor outputs [29]. With the diameter of the taxel set to 4 mm, we used indenters of different sizes and shapes to test how they affected the grayscale value response of the taxels. We used circular indenters with diameters 3, 4, 5, and 6 mm and square indenters with side lengths 3, 4, 5, 6, and 12 mm. Applied pressure versus the grayscale value of a single taxel for each indenter was recorded three times and the average values were taken (Fig. 4(d)). The results indicate that the response varies with the indenter size and converges towards a specific response as the indenter size gets larger with the response for 6 mm × 6 mm being close to that for 12mm × 12mm. Smaller indenters result in non-uniform pressure application causing the grayscale values to deviate noticeably compared to large indenters approximating uniform pressure application. This also implies that the accuracy of pressure estimation during general operation will depend on the feature sizes of the contacts with the sensor.

V. Design and Fabrication of Tactile Sensor Module

Based on the optimized design of the piezoluminescent skin realized above, we developed a large area cylindrical tactile sensing module for application to robotic manipulators. Fig. 5(a) illustrates the design of the cylindrical tactile sensor. The base of the sensor module is a 3D-printed structure that houses the camera. It also contains an annular groove of 3 mm gap

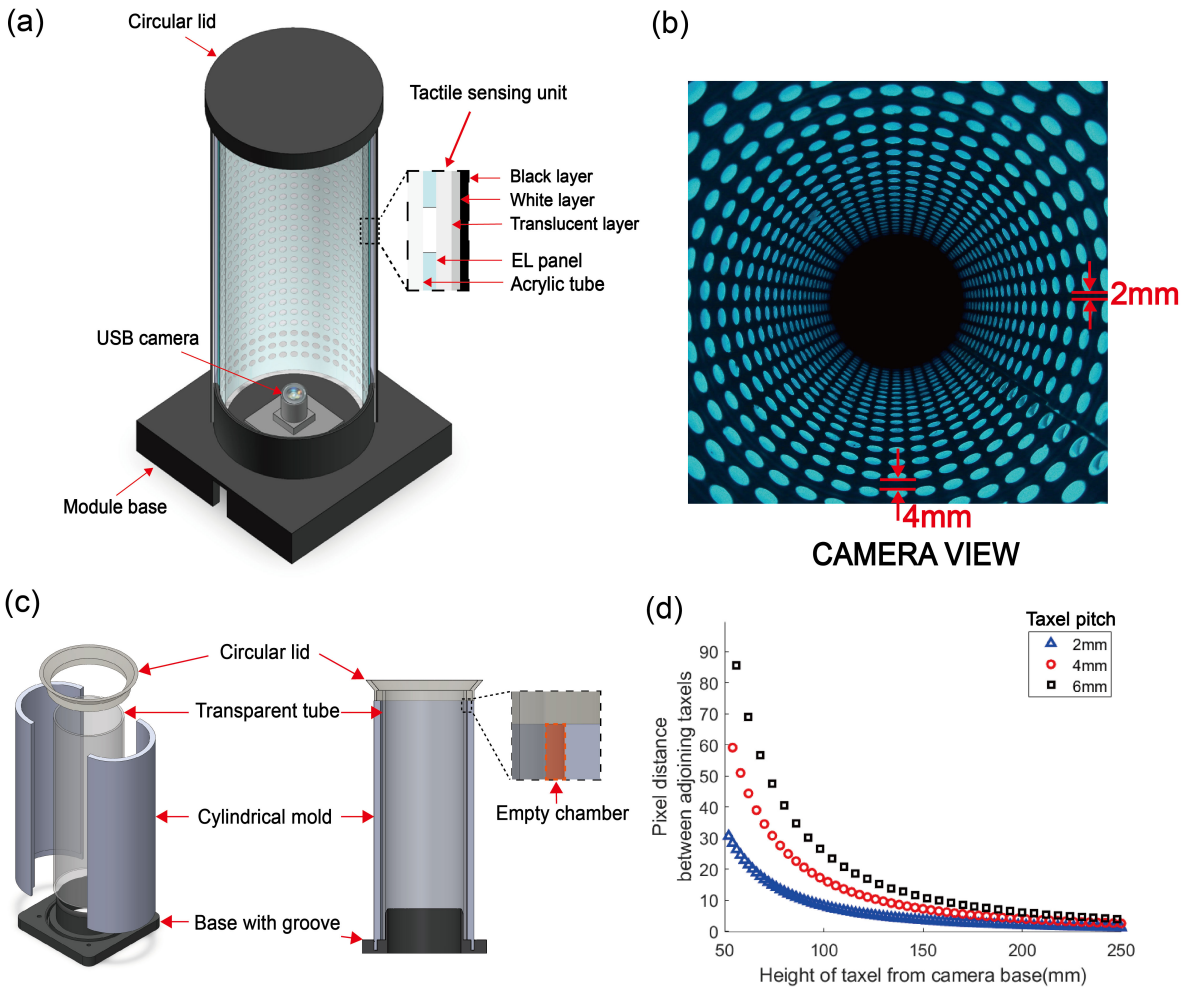

Fig. 5. (a) Illustration of a large area cylindrical tactile sensor based on the piezoluminescent skin. (b) Image captured by the internal camera when the EL panel is activated. Each blue circle represents a taxel. (c) Casting mold for fabrication of laminated multi-layer piezoluminescent skin. (d) Simulation results of the pixel distance vs height from the camera base for different taxel pitches.

to hold the sensor structure. A cylindrical transparent acrylic tube with an outer diameter of 80 mm and a thickness of 2.5 mm covered by the piezoluminescent skin is affixed in the annular groove in the base. The transparent acrylic tube serves as the skeletal structure of the sensor providing load-bearing capacity and also allows the transmission of light from the piezoluminescent skin to the camera. A seamless multilayered piezoluminescent skin of a total thickness of 4 mm is affixed over the transparent acrylic tube.

The innermost layer of the piezoluminescent skin is a 300 μm thick EL panel measuring 210 mm $\times$ 297 mm. An array of circular apertures of diameter 4 mm are made into the panel using a CNC milling machine. Consecutive apertures have a horizontal space (edge to edge) of 2 mm and a vertical space of 4 mm between them. The EL panel with the apertures is wrapped around the acrylic tube and attached to it using superglue. Then, a cylindrical multi-layered elastomer structure consisting of a translucent transmitting layer, a white reflecting layer, and a black opaque layer is fabricated separately and affixed over the transparent acrylic tube attached to the EL panel. Positioned at the uppermost section of the cylinder is an opaque lid to prevent external environment light from interfering with the camera images. The base of the sensor houses a USB camera (ELP-USB4KHDR01, Sony IMX317) with a 2.1 mm lens operating in 1080p 30 FPS mode. The camera is used to enable real-time monitoring of light intensity of the entire inner surface of the transparent cylinder. Fig. 5(b) shows an image of the internal surface of the tactile sensor as viewed by the USB camera, where each luminous blue circle is one taxel.

A. *Design of Taxel Layout*

For the cylindrical tactile sensor module, the distribution layout of the taxels is crucial to distinguish individual taxels far from the camera and obtain optimal spatial resolution. Each circular aperture on the EL panel represents a tactile unit or a taxel. Ideally, a higher density of taxels per unit area indicates a higher localization resolution and a lower TPD distance achievable by the tactile sensing system. However, due to limitations in camera resolution and the camera's non-

vertical alignment with the EL panel, regions farther from the camera occupy smaller areas in the captured image. Thus, it is necessary to consider that if taxels are too dense or the diameter is too small, some taxels may not be recognized independently in the image, leading to overlapping areas and compromising recognition accuracy. We set that the pixel distance between each taxel in the image should be greater than 3 to ensure the distinction between the taxels during image processing and conduct a simulation to calculate the suitable spacing between apertures on the EL panel.

The initial step is to obtain the camera calibration model. This process includes obtaining a sufficient number of 3D spatial points within a predetermined world coordinate system and ascertaining the corresponding pixel coordinates of these points in the image. This establishes a correlation between the world coordinates and the image coordinates [36]. Considering that the taxels are at a radial distance of 40mm, which is equal to the diameter of the acrylic tube, we utilized the camera model and calculated the pixel distance in the image for taxels with vertical spacings of 2 mm, 4 mm, and 6 mm at different vertical distances from the camera. Fig. 5(d) shows that for a specific taxel distance, the pixel distance between two adjoining taxels decreases as we move further away from the camera. For a tactile sensor of a height of 200 mm from the camera base, a vertical distance of 4 mm between pixels ensures that each taxel in the image has an appropriate pixel distance of 4. A smaller vertical distance of 2 mm will lead to a pixel distance of 2 at 200 mm height. Thus, we fix a vertical distance of 4 mm between taxels for our sensor design. For horizontal spacing between taxels, there is less issue with overlapping taxels in the image as can be seen in Fig. 5(b); so we chose a horizontal spacing of 2 mm.

B. Fabrication of Cylindrical Piezoluminescent Skin

We developed a casting method for fabricating a seamless laminated structure of the elastomeric skin for the cylindrical tactile sensor. The design of the mold is shown in Fig. 5(c). The 3D-printed base contains a cylindrical groove in which the transparent acrylic cylinder that forms the inner part of the sensor is inserted. Two 3D-printed semi-cylindrical molds are aligned and inserted into the groove on the base. The dimensions are such that a cylindrical air gap of 2 mm is left between the 3D-printed mold and the acrylic tube. Ecoflex 00-30 pre-cure mixture diluted with silicone thinner is degassed and poured into the gap between the cylinder mold and the transparent acrylic cylinder using a circular lid as a funnel. This is left to cure for 4 hours resulting in the first layer of the elastomer structure formed over the acrylic tube. Next, the set of semi-cylindrical molds is replaced by another with inner diameter increased by 2 mm and the mixture for white reflecting layer with 1% white pigment is cured in the chamber. Finally, the semi-cylindrical molds are replaced by a third set with a further increased inner diameter by 2 mm and Ecoflex 00-30 mixed with 1% black pigment (Silc Pig, Smooth-On) is cured in the chamber. After demolding, a three-layered elastomer structure with a translucent inner layer, a reflective white middle layer, and an opaque black outer layer and a total thickness of 4 mm is obtained. The three layered structure is carefully removed from the acrylic tube and inserted over an acrylic tube with the EL panel of dimensions 210 mm $\times$ 297 mm affixed to it. This fabrication method enables the preservation of a small air gap between the acrylic tube and the translucent layer, allowing the elastomer to deform at lower pressure enhancing the sensor's sensitivity.

VI. Model and calibration

The fabricated cylindrical tactile sensing module requires two types of calibration in order to be employed for contact localization and pressure estimation. The first involves establishing a camera model to map each pixel in the image to its corresponding location in the real world. The second involves identifying the mapping between the intensity of a taxel in the image to the normal pressure applied on it in the real world.

A. Camera model

To achieve the conversion from 2D-pixel coordinates on the image plane to 3D world coordinates, camera calibration is required. Camera calibration involves obtaining a sufficient number of spatial points in a known world coordinate system, finding the corresponding 2D-pixel coordinates of these points in the image, and establishing the correspondence between the world coordinates and the image coordinates (Fig.6).

To facilitate coordinate transformation, we establish a three-dimensional coordinate system called the camera coordinate system (X_c, Y_c, Z_c) with the origin at the camera's optical center and the z-axis coincident with the camera's optical axis. The optical center is at a distance of f (the focal length of the camera lens) from the image sensor. We also set up a plane coordinate system called the image coordinate system (X_p, Y_p) in the plane of the image sensor such that The Z_c axis passes through the origin of the image coordinate system. Since the pixel origin of the captured image is in the top-left corner, we establish a pixel coordinate system (U, V) with the origin at the top-left corner of the image coordinate system. The pixel coordinate system is coplanar with the image coordinate system.

Assuming a point P on the cylinder has coordinates (x_c, y_c, z_c) in the camera coordinate system, we can project point P onto the image coordinate system along the P-Zc direction, resulting in the coordinates $P_2(x_p,\ y_p)$ in image coordinate system. Since the image coordinate system is parallel with the pixel coordinate system, we can obtain the coordinates $P_3(u,\ v)$ from point P_2. By applying the principles of similar triangles based on geometric relationships, we can derive

$$z_c x_p = f x_c, z_c y_p = f y_c \tag{1}$$

Converting equation (1) to matrix form, we obtain:

$$z_c \begin{bmatrix} x_p \\ y_p \\ 1 \end{bmatrix} = \begin{bmatrix} f & 0 & 0 \\ 0 & f & 0 \\ 0 & 0 & 1 \end{bmatrix} \begin{bmatrix} x_c \\ y_c \\ z_c \end{bmatrix} \tag{2}$$

Using equation (2), we have accomplished the transformation between the camera coordinate system and the image

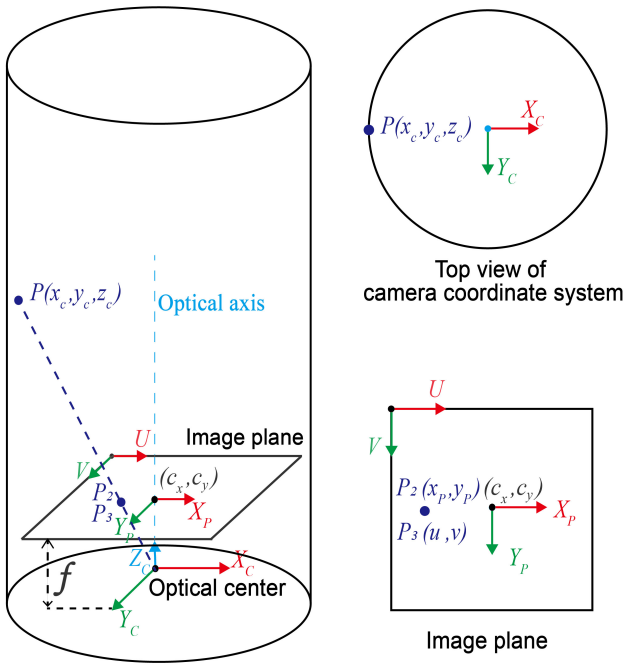

Fig. 6. Camera calibration model, X_c, Y_c, and Z_c axes coincide with the optical center. The camera focal length is known to be f = 2.1 mm, and the pixel size is d_x = 2.2 µm and d_y = 2.2 µm.

coordinate system. Additionally, considering that U is aligned with the X_p axis and V is aligned with the Y_p axis, (c_x, c_y) represents the coordinates of the image coordinate system's origin, and d_x and d_y denote the actual horizontal and vertical physical dimensions of each pixel, we can calculate

$$u = c_x + x_p/d_x, v = c_y + y_p/d_y \tag{3}$$

Converting equation (3) to matrix form, we obtain:

$$\begin{bmatrix} u \\ v \\ 1 \end{bmatrix} = \begin{bmatrix} \frac{1}{d_x} & 0 & c_x \\ 0 & \frac{1}{d_y} & c_y \\ 0 & 0 & 1 \end{bmatrix} \begin{bmatrix} x_p \\ y_p \\ 1 \end{bmatrix} \tag{4}$$

By substituting equation (2) into equation (4), we obtain

$$\begin{bmatrix} u \\ v \\ 1 \end{bmatrix} = \frac{1}{z_c} K \begin{bmatrix} x_c \\ y_c \\ z_c \end{bmatrix} \tag{5}$$

in which the camera's intrinsic matrix, K is given by:

$$K = \begin{bmatrix} \frac{f}{d_x} & 0 & c_x \\ 0 & \frac{f}{d_y} & c_y \\ 0 & 0 & 1 \end{bmatrix} \tag{6}$$

The transformation from the pixel coordinate system to the world coordinate system is given by:

$$\begin{bmatrix} x_c \\ y_c \\ z_c \end{bmatrix} = z_c K^{-1} \begin{bmatrix} u \\ v \\ 1 \end{bmatrix} \tag{7}$$

The K can be obtained using the camera calibrator app in MATLAB's Computer Vision Toolbox™.

$$K = \begin{bmatrix} 996.6227 & 0 & 965.2231 \\ 0 & 991.0198 & 579.5909 \\ 0 & 0 & 1 \end{bmatrix} \tag{8}$$

As the piezoluminescent skin is wrapped around the acrylic cylinder of fixed diameter, this places a constraint making the real-world coordinates for any point on the skin, x_c and y_c dependent on each other. By combining equations (7) and (8) with the equation $x_c^2 + y_c^2 = R^2$, where R represents the radius of the cylinder (40 mm), and substituting the pixel coordinates, we can determine the unique solution for the 3D coordinates in the camera coordinate system, with the optical center as the origin. From the matrix K identified for our camera, it can be observed that f/d_x and f/d_y are 996.6227 and 991.0198, respectively. Given a pixel size of 2.2 µm × 2.2 µm, the calculated focal length f is approximately 2.18 mm, which aligns closely with the 2.1 mm lens chosen for the camera.

B. Pressure calibration

In the cylindrical tactile sensor module, each taxel has a unique coordinate relative to the optical center. Taxels at different z-coordinates result in different viewing angles from the camera. Furthermore, the solid angle subtended by taxels at different z-coordinates at the camera lens are also different. Due to these reasons, the initial light intensity of taxels as captured in the camera image is non-uniform and the area occupied by each taxel in the image depends on its z-coordinate. We first study how the light intensity of the taxels is influenced by the distance and the viewing angle of the light receptor. For this, we took an EL panel of dimensions, 110 mm × 70 mm, and used a light meter for measuring the light intensity at varying distances and viewing angles. We fix the light meter probe at a specific distance from the center of the panel with the probe directly facing it. Then, the probe is moved around in an arc subtending different angles from 0 to 180 degrees to the surface of the EL panel. The experimental environment was kept dark to minimize the influence of environmental light.

In Fig.7(a), illuminance measured by the light meter for changing viewing angles at three different distances from the EL panel is shown. For a fixed distance(10 cm, 20cm, or 30 cm) and varying the angle between the light meter probe and the EL panel, the light meter always receives peak light intensity when the probe is orthogonal to the surface. As the angle to the surface decreases, the illuminance received by the probe decreases. Additionally, under a fixed angle, reducing the distance significantly increases the light intensity. Therefore, it is essential to consider the relationship between the light intensity and the distance of the taxels from the camera for pressure calibration.

To calibrate the cylindrical tactile sensor, we collected data of six taxels at different vertical distances from the camera. By manually probing the sensor surface with a 2 mm cylindrical indenter while observing the camera feed, we marked the locations on the outer surface corresponding to the selected

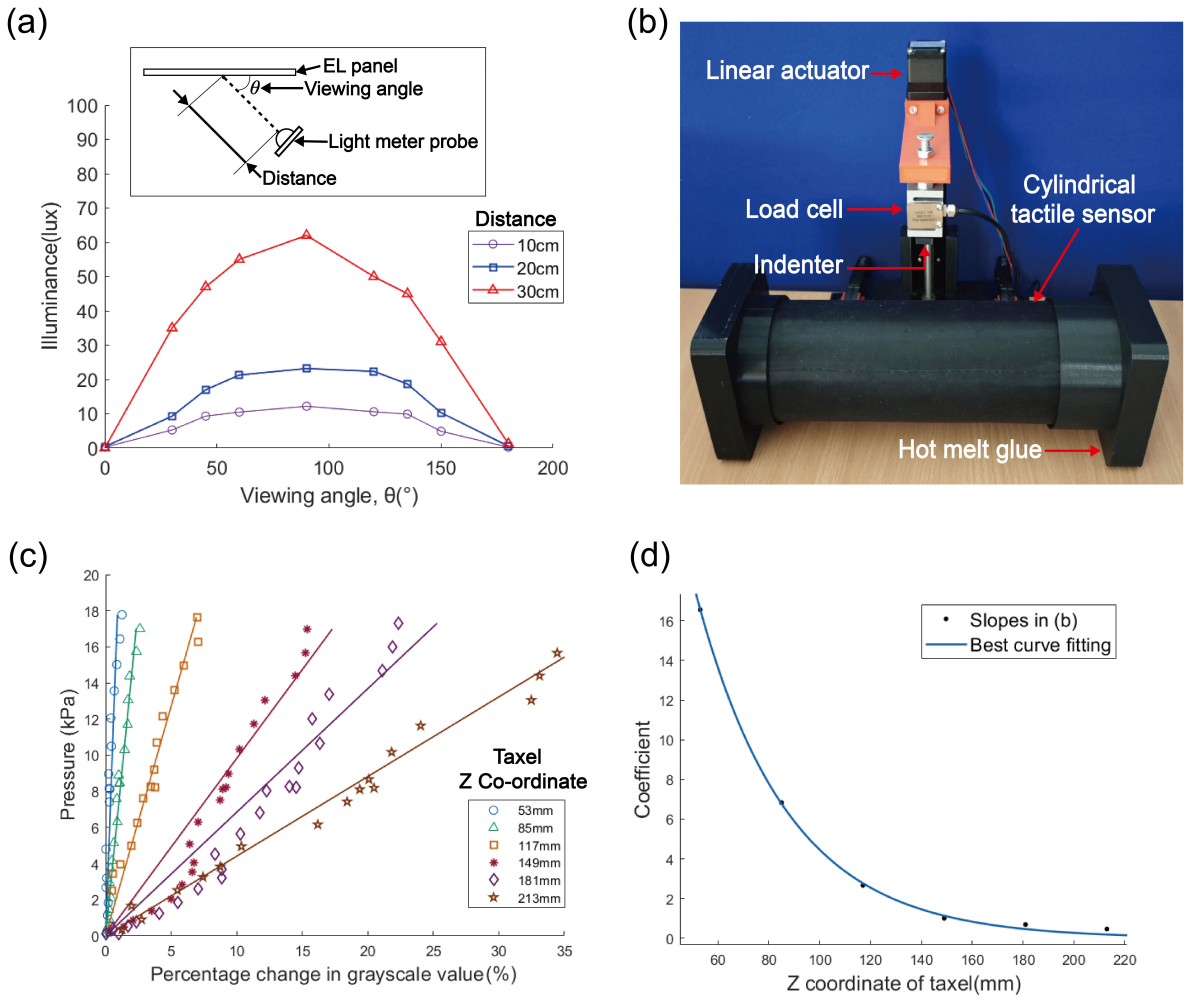

Fig. 7. (a) Illuminance vs viewing angle at different distances from the EL panel. (b) Experiment platform for calibration of cylindrical sensor. (c) Percentage of grayscale value vs pressure (0-20 kPa) for taxels at different Z coordinates taxels in the camera coordinate system. The solid lines represent linear-fitted curves. (d) The linear coefficients are plotted against the Z coordinates of taxels and fitted with the exponential function.

taxels. A 12 × 12 mm indenter was fixed to the load cell mounted on a motorized lead screw as illustrated in Fig. 7(b). The linear actuator with a load cell attached to it was firmly secured to the table using two table clamps. To capture the data for each of the selected taxels, the tactile sensor's position was manually adjusted to align the indenter precisely with the corresponding marked location on the sensor surface and affixed to the table with hot melt glue. As the indenter area is larger than that of a single taxel, it completely covers the projected area of the target taxel on the outer surface during data collection. The tactile sensing skin was then indented with a displacement increment of 0.05 mm per step For each displacement step, the force measured by the load cell was recorded and divided by the area of the indenter to calculate the pressure ($P = F/S$). Subsequently, the sum of grayscale values from the taxel was recorded three times and averaged to obtain the sum of grayscale values within the taxel corresponding to the pressure. For each compression step, the difference in averaged sum of grayscale values within the taxel was expressed as a percentage of its initial value before the application of pressure. This process was continued until the force measured by the load cell reached a maximum set value corresponding to a pressure of 20 kPa.

In Fig. 7(c), the data from six taxels at different heights(corresponding to different Z coordinates in the camera coordinate system) for the range of 0 to 20 kPa are shown. While the change in the magnitude of grayscale values to applied pressure is lower for taxels farther from the base, the percentage change is larger due to a lower initial brightness of these taxels. A linear curve fit function, $P(I) = cI$, was used to fit the relation between the pressure P applied and the percentage change in grayscale value, I for each of the six taxels tested. The average R-squared value for these six curves representing the taxels at different Z coordinates is 0.892. The coefficient c is dependent on the Z coordinate of taxels, and is modeled by an exponential function $c(Z) = a \cdot e^{bZ}$ (Fig. 7(d)). The coefficients a and b determined from curve fitting are 72.75 and -0.02792 respectively. By utilizing the fitted function $P(I) = c(z)I$, We can estimate the pressure on any taxel by substituting the percentage change in its grayscale

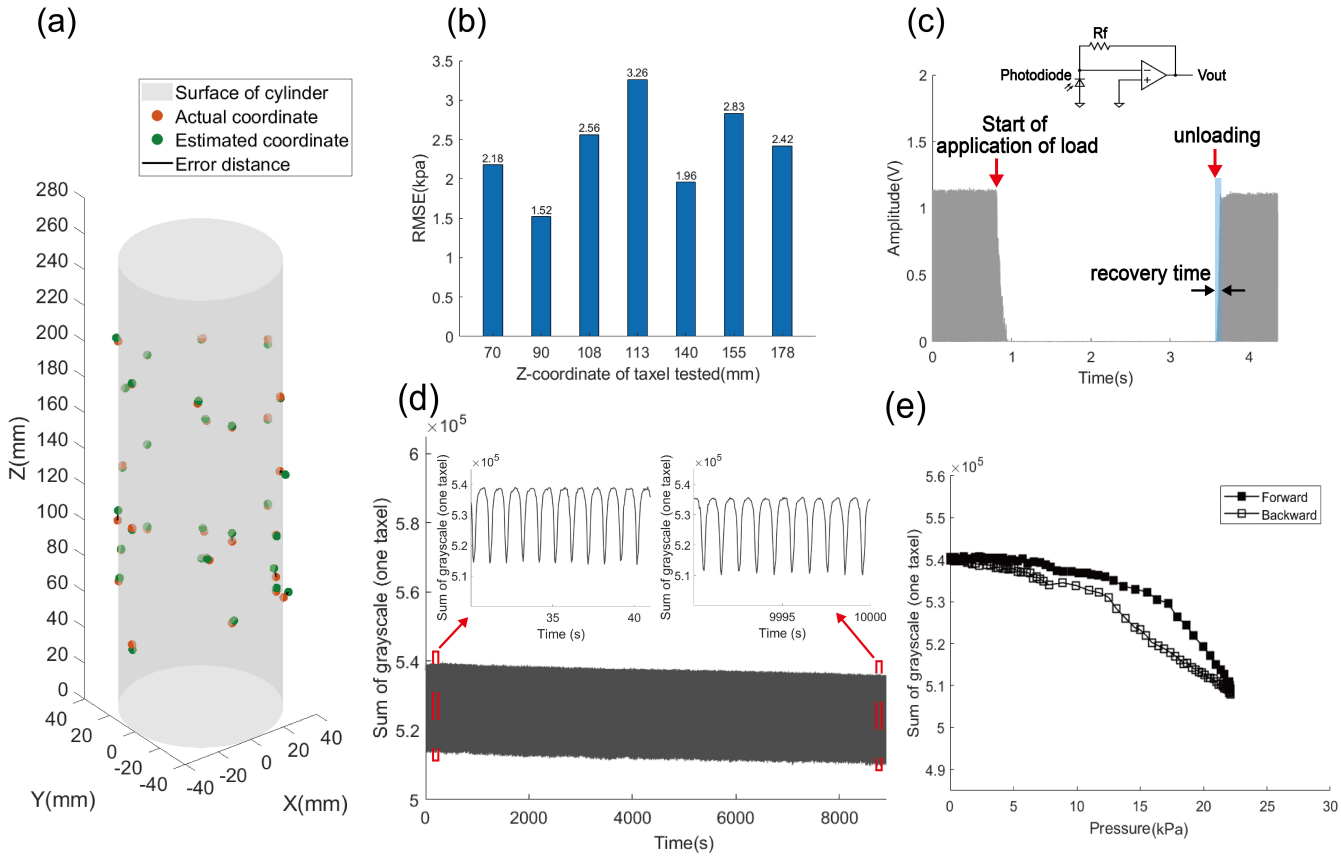

Fig. 8. (a) Localization accuracy. Orange points indicate the actual location and green points indicate the estimated location with black lines connecting each pair of corresponding data points (b) Pressure-estimation RMSE at different heights from the base. (c) Recovery time measured from a single taxel. (d) Repeatability testing of piezoluminescent skin over 10,000 cycles. (e) Hysteresis testing of piezoluminescent skin at 0.5 mm/s strain rate.

value.

C. Contact localization and pressure estimation

Once the cylindrical tactile sensor is calibrated, the procedure for localizing applied pressures and estimating their magnitude is as follows. An initial image without any application of pressure on the sensor is captured and a grayscale threshold is applied to obtain a 2D mask and each connected region in the mask is initialized as a taxel. The percentage change in the average grayscale value of each taxel between the initial and current image is computed and the pressure magnitude is estimated using the pressure calibration model. Utilizing this normalized metric for calibration mitigates the impact of minor variations in taxel areas within the image. Given the influence of noise in low-light conditions, we set the minimum detectable pressure as 6 kPa. The centroid coordinates of the taxels with pressure exceeding the set threshold are transformed into world coordinates using the camera calibration model and plotted along with a colormap to indicate the pressure magnitude at each point.

VII. Sensor Characterization and Demonstration

After realizing the calibration of the cylindrical tactile sensor, we characterize its various performance metrics such as localization accuracy, TPD distance, pressure-estimation accuracy, and response time.

A. Localization Accuracy

To characterize the localization estimation accuracy of the designed sensor, we used a 6 $\times$ 6 mm indenter with a square cross-section. While we conducted sensor calibration using an indenter with 12 $\times$ 12 mm, we used an indenter with a smaller cross-section to avoid activating multiple taxels at the same time. We randomly sampled 30 points on the sensor and pressed them with the indenter, recording the probe's central point as the location of the pressure application. In Fig. 8(a), the orange points represent the actual world coordinates of the touch points we measured, the green points indicate the world coordinates calculated and output by the sensor, and the black lines are used to connect these two points for each sample to indicate the distance error. The overall Root-Mean-Square Error (RMSE) for this test is 1.92 mm indicating a high localization accuracy of this sensor.

B. Pressure Estimation Accuracy

To assess the accuracy of pressure estimation, considering the varying angles and distances between the taxels and the

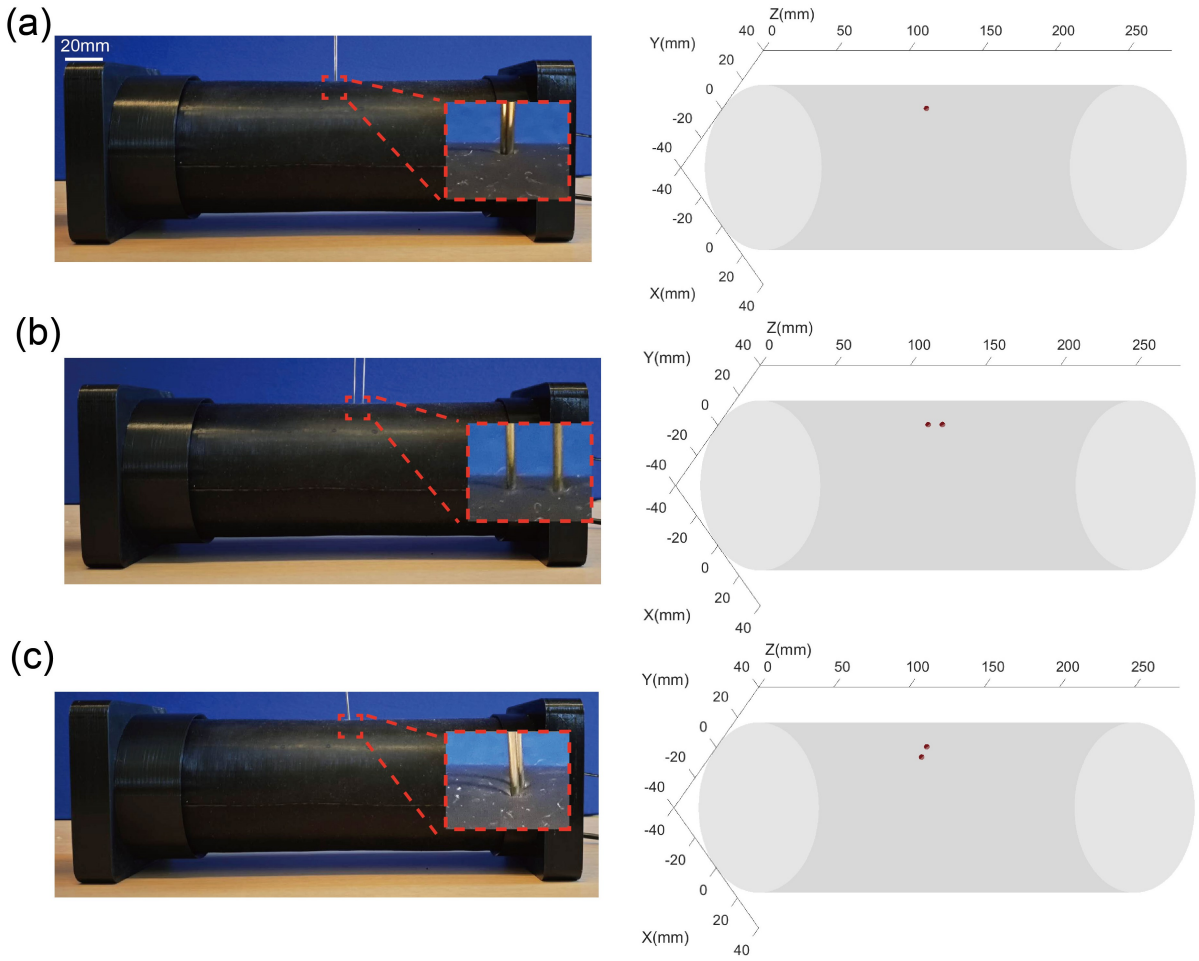

Fig. 9. Two-point discrimination distance test. (a) Two indenters of 1 mm diameter are attached together and pressed against the sensor at one point registering a single contact point in the sensor output. (b) The two indenters are moved 3 mm apart along the Y-axis and pressed against the sensor registering two points in the sensor output. (c) The two indenters are moved 5 mm apart along the Z-axis and pressed against the sensor registering two points in the sensor output.

camera at different heights, we performed tests at seven distinct heights using a 12 mm × 12 mm indenter. At each height, we randomly selected five points for testing. By utilizing a linear actuator equipped with a load cell, we applied pressures within the range of 6 kPa to 20 kPa, and the camera images were utilized to compute the estimated pressures. The RMSE for all 35 test points is 2.45 kPa. The estimation errors are plotted against the height of the taxels in Fig. 8(b). We observe that even at different heights, the resulting RMSE values are in a similar range, indicating that our sensor exhibits good consistency and accuracy in pressure estimation at different heights.

C. Response Time

The response time of our tactile sensor is related to two aspects- the viscoelastic behavior of the elastomeric skin and the frame rate of the camera. Utilizing the experimental platform illustrated in Fig. 3(b), we conducted experiments to assess the maximum detectable frequency of tactile events by the tactile skin. A square tactile skin sample was placed on the acrylic board and the light meter was replaced by a photodiode (Vishay, BPW20RF) with a faster sampling rate than the light meter and the camera. This modification is aimed at precisely evaluating the response time required for compression deformation and recovery time for elastomer to rebound. To isolate the signal interference from the high-frequency driving current of the EL panel, we utilized a 3 mm core diameter (4 mm outer diameter) optical fiber to transmit the light signal to the photodiode placed outside the testing platform. As a high-frequency AC signal of over 800Hz generated by the inverter is used to drive the EL panel, the panel generates a corresponding frequency of the light signal, resulting in the fluctuating values detected by the photodiode. The average amplitude of the signal corresponds to the total light intensity emitted from the taxel.

We manually apply a load to the skin sample by pressing manually with an indenter to achieve an approximate deformation of 2.5 mm. The output of the photodiode reduces close to 0V upon application of the load. After waiting for a short time, the load is rapidly removed simulating a step signal for unloading. The photodiode signal took approximately 33.85 ms to rise from 0% to 90% of its final output, representing

the 90% steady-state response time which we also refer to as the recovery time (Fig. 8(c)). When the force application matches the sensor's recovery speed, the total time for both application and recovery is around 67.7 ms. This indicates that our designed tactile skin can detect tactile events with a compression deformation of 2.5 mm approximately 15 times within one second. This indicates that our designed tactile skin can detect tactile events with a compression deformation of 2.5 mm approximately 15 times within one second. The camera with a frame rate of 30 FPS used in the sensor system meets the requirement for detecting a maximum of 15 touch events per second. As we applied a relatively large compression of 2.5 mm manually for measuring the response time, it can be inferred that the response time for tactile events corresponding to deformations lower than 2.5 mm may be smaller and the use of a camera with a higher sampling rate can improve the bandwidth of the sensor.

D. Hysteresis and repeatability test

We utilized the experimental platform depicted in Fig. 4(b) and employed a camera as the light intensity signal receiver to observe the hysteresis performance of a single taxel. A 12 mm $\times$ 12 mm square-shaped indenter was affixed to the load cell, and a strain rate of 0.5 mm/s was used to apply pressure ranging from 0 to 20 kPa. The experiment was conducted for ten cycles and the data from the last cycle was taken, with the results shown in Fig. 8(e). We evaluated the hysteresis loss as 19.2% [37].

To evaluate the repeatability of the piezoluminescent skin, we used the same experimental setup as for the hysteresis measurement to observe the response drift of a single taxel under repeated loading. We applied a total of 10,000 cycles, with the results shown in Fig. 8(d). The difference between the average peak values from the first 10 cycles and the last 10 cycles was calculated and divided by the average amplitude of the first 10 cycles to express the sensor drift as a percentage. The light intensity response shift of the taxel was evaluated to be approximately 12.9%.

E. Two-point Discrimination Distance

As shown in Fig. 2(b), the TPD distance of our sensor is related to the distance between two taxels. We utilized two cylindrical indenters with a circular cross-section of 1 mm diameter for evaluating the TPD distance. The two indenters were first placed closely together on the sensor applying pressure. The sensor output shows only a single detection point as shown in Fig. 9(a). Then we gradually increased the distance between the two indenters and recorded the separation distance when the sensor's feedback showed a transition from one detection point to two points in the sensor output as seen in Fig. 9(b)). This distance is considered to be the TPD distance. Given the different horizontal and vertical distances between taxels in our tactile sensor (2 mm and 4 mm respectively), the test results showed a vertical TPD distance of approximately 5 mm, while the horizontal TPD distance is 3 mm(Fig. 9(b, c)).To further evaluate the sensor's performance, we conducted experiments for regions at distances of 50 mm and 200 mm from the camera. The results demonstrated that for the region at 50 mm height from the camera, the vertical TPD distance was approximately 4 mm and the horizontal TPD distance was 3.5 mm, while at 200 mm, the vertical TPD distance increased to 6 mm and the horizontal distance to 4 mm. These results indicate that our sensor maintains a consistently low TPD distance over a wide detection range.

F. Multi-point Contact Detection and Pressure Estimation Demo

The calibrated sensor can be utilized for both single and multi-point touch detection. Illustrated in Fig. 10(a), when an operator simultaneously touches the sensor with five fingers, and the distance between the fingers exceeds the TPD distance, the sensor indicates five distinctly separate regions in the visualization of the result from the sensor. The pressure on each taxel is depicted by a color whose magnitude is shown by the accompanying pressure map. Due to the contact area between the individual fingers and the skin exceeding the area of one 4 mm diameter taxel, multiple taxels within a connected region are activated showing a detailed pressure map for each contact. *Supplementary Video 1* shows feedback of pressure in multi-point contact scenarios. The points that experience applied pressures over 6 kPa are depicted in different colors with their pressure magnitude corresponding to the values shown in the colormap. Furthermore, when a spring is compressed against the sensor surface and released slowly, the color of the pressure indicator changes from red to orange to blue indicating a gradual reduction in the magnitude of pressure at that point.

G. Robot guidance based on tactile sensing module

One of the key applications envisaged for the tactile sensor module is to enable intuitive human-robot guidance by acting as a sensor interface mounted on a robot for humans to interact with. To demonstrate the potential for this application, we have integrated the tactile sensor module as the end-effector of a 6-dof collaborative robot (Inovo Modular Robotic Arm, Inovo Robotics Ltd., United Kingdom) and demonstrated a simple guidance operation (Supplementary Video 2).

To realize this guidance, we first evaluate the vector sum of the forces applied on the sensor based on the pressure estimated by the taxels to obtain the desired direction of motion. Let us consider that the pressure estimate of the i^{th} taxel is given by $P^i_{(x_c,y_c,z_c)}$ and assume that uniform pressure is applied across the taxel area, A_{taxel}, including on the rectangular boundary around the circular aperture (5mm $\times 6mm$). As we know the pressure is applied normally to the sensor surface pointing radially towards the cylindrical axis, the direction of the force is given by the unit vector $(-x_c, -y_c)/\sqrt{x_c^2 + y_c^2}$. The vector sum of the force on all taxels is given by:

$$\vec{F}_{sum} = \sum_{i=1}^{n} \frac{(-x_c, -y_c)}{\sqrt{x_c^2 + y_c^2}} \cdot P \cdot A_{taxel} \tag{9}$$

where n is the number of taxels. The pressure of all taxels with estimated pressures less than 6 kPa are set to zero to

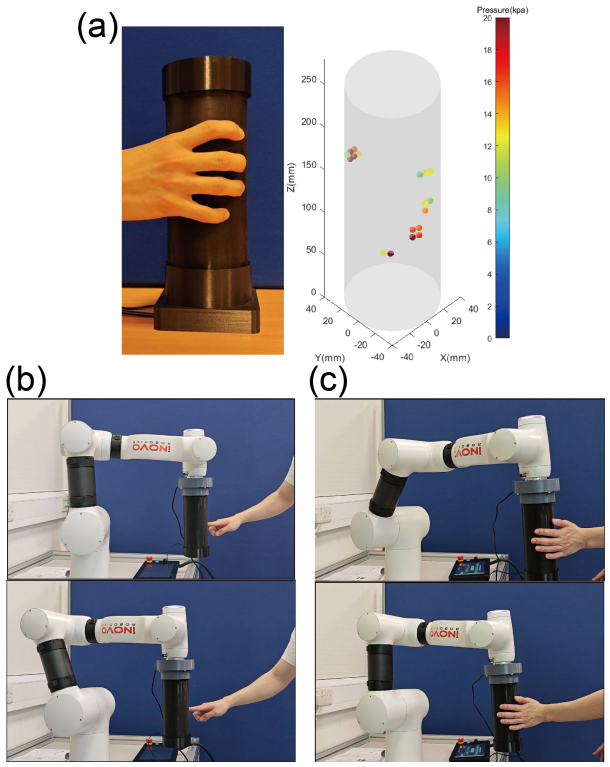

Fig. 10. Demonstration of tactile sensing module. (a) The multi-point touch sensing with the visualization shows detected contact points with their pressure magnitude represented by the colormap. (b) Robot arm guidance using a single finger. (c) Robot arm guidance using one hand.

avoid unintended movements due to sensor noise. The force computed is with reference to the camera coordinate system. This is then transformed into the wrist coordinate system. The position of the wrist of the robot is updated based on zero-stiffness admittance control. As a result, the robot moves in the direction of the applied force in the plane of the image sensor with a constant velocity until the applied force is present and stops when the applied force is removed.

As illustrated in Fig. 10(b), and Fig. 10(c) and Supplementary Video 2, an operator uses a single finger and the palm to make contact with the tactile sensor mounted on the Inovo robot arm and gently guide it to move along a desired direction in the XY plane of the sensor coordinate system.

VIII. Discussion

A. Comparison with Other Large Area Tactile Sensors

We first discuss the pressure estimation accuracy of large area tactile sensors in literature. The TacLINK utilizes a deformable elastomer structure pressurized internally and tracks the deformation of internal markers. Due to this, the force sensitivity and accuracy are dependent on the internal air pressure [14], [38]. Under conditions of low internal air pressure, such as 0 kPa, the estimated force exhibits negligible deviation from the actual force. However, due to the low internal air pressure, there is a limitation on the system's load-bearing capacity. As the internal air pressure gradually increases, the difference between the force signal from the probe and the force signal output from the sensing system becomes higher. At an internal air pressure of 1.5 kPa, a force of 1.35 N was applied with a 5.5mm diameter indenter while TacLINK's estimate was 0.55 N yielding an approximate pressure estimation error of 33.7 kPa [14]. The force estimation errors for ERT-based large area tactile sensors fall within the range of 2.00 N ± 1.18 N, representing approximately 20% of the maximum detection force (10 N) [39]. In our sensor, the RMSE for pressure estimation is approximately 2.45 kPa over the proposed measurement range of 6-20 kPa. The rigid platform for mounting the piezoluminescent skin coupled with the direct correspondence between the light intensity and pressure magnitude decreases computational complexity while also retaining load bearing ability of the sensor structure.

Regarding spatial resolution, TacLINK has a lateral surface area of 577.76 cm^2, having a total of 240 sensing regions. The calculated density of sensing units amounts to approximately 0.415 taxels per square centimeter. Similarly, VTacArm has a total marker count of 250 on the skin with a lateral surface area of 274.75 cm^2. The computed sensing unit density stands at 0.91 taxels per square centimeter [14], [26], [38]. In our sensor design, the camera with the 2.1 mm lens captures 782 taxels within its viewing area. The overall lateral surface area of the sensor is 502.40 cm^2 and the calculated taxel density is 1.557 taxels per square centimeter. It is noteworthy that our average taxel density is constrained due to the limitations of the lens's capturing angle and the potential substitution of the lens with a broader field of view could further improve the sensor's effective detection area. Benefiting from a heightened distribution density of taxels, the sensor we designed resulted in a localization RMSE of 1.92 mm. In ERT-based methods, spatial resolution is related to the quantity and configuration of electrodes as well as the number of data points used to calibrate or train the localization model. In the works with electrodes incorporated at the sensor's center, the localization accuracy typically ranged from 3.9 ± 2.7 mm to 28.5 ± 10.2 mm [20], [33], [39]–[43].

There are electronic sensor skins that adopt modular designs and are scalable, such as the ROBOSKIN and Hex-o-skin [29], [44]. The shape of each flexible PCB sensor module is that of an equilateral triangle with an area of 3.9 cm^2. Each module has 12 round pads serving as taxels and a capacitance-to-digital converter. Intercommunication between each triangular module is achieved through an I^2C serial bus, with every 16 modules requiring a microcontroller board for communication with the PC via the CAN bus. To achieve the same detection area as our proposed sensing system, the ROBOSKIN would require approximately 128 modules and 8 MCUs. Compared to our design, the modular iCub robot skin offers a higher taxel density and a faster sampling rate.

In practical applications, such as on a robotic arm, it requires an additional framework layer on the existing arm surface, along with enough space to house the analog-to-digital converter behind the tactile sensor module [29], [44]. While vision-based tactile sensors can be easily integrated to the wrist of a robotic arm, serving as an extra link, replacing a robotic

TABLE I
COMPARISON WITH RELATED WORKS

Reference	Method	Localization error	Taxels / cm^2	TPD distance	Sampling rate	Measuring range	Hysteresis
Lee et al. [40]	ERT-based	28.5 ± 10.2 mm	0.5626	/	200Hz	/	/
Lee et al. [41]	ERT-based	78.5% hit rate	/	/	/	0 to 10 N	4.7%
Park et al. [20]	ERT-based	5.2 ± 3.3 mm	0.9554	/	120Hz	/	/
Lee et al. [39]	ERT-based	8.13 ± 4.32 mm	0.81	35 mm to 55 mm	/	0 to 10 N	8.3 ± 4.7%
Park et al. [33]	ERT-based	3.9 ± 2.7 mm	1.2346	/	12.5kHz	/	/
Park et al. [42]	ERT-based	6.6 ± 3.5 mm	0.6336	/	110Hz	0 kPa to 18 kPa	20%
Lee et al. [43]	ERT-based	74.4 mm	0.2658	/	30Hz	4.9 N to 9.81 N	/
Zhang et al. [26]	Marker-tracking	/	0.91	/	40Hz	/	/
Luu et al. [38]	Marker-tracking	7.19 ± 1.06 mm	0.415	140 mm	120Hz	/	/
Schmitz et al. [29]	Capacitive	/	3.0769	1 mm to 10 mm	100Hz	0 to 700 kPa	/
Mittendorfer et al. [44]	Optical	/	0.5882	/	1kHz	/	/
Fu et al. [28]	EL panel-based	6.63 mm	0.45	/	30Hz	3.1 to 9.4 N	23.8 to 28.2%
This paper	EL panel-based	1.792 ± 0.997 mm	1.557	3 mm(vertical) & 5 mm(horizontal)	30Hz	6 to 20 kPa	19.2%

arm's link is challenging. Transparency between the taxels and the camera is essential and the camera must be able to capture the light intensity changes in the taxels, implying that this system might require a higher degree of customization compared to electronic tactile sensing methods. In addition, realizing vision-based sensing for largely curved structures is also challenging because it is difficult to design an imaging system to achieve coverage of all regions.

Studies involving variable stiffness links based on pressurized elastomeric shells as well as tactile sensing robot links based on marker tracking methods have realized robot manipulators with hollow internal structures [45]–[47]. These works provide a valuable reference for incorporating tactile sensing based on vision while retaining other components needed for the functionality of robot arms.

In terms of TPD distance, the human forearm's normative TPD values in an 18-year-old typically range from 27.41 mm to 30.09 mm, while fingertips exhibit lower TPD values, ranging from 4.76 mm to 6.55 mm [48]. In sensors based on visual methods and using the markers tracking technique, the achieved TPD distance is approximately 140 mm [38]. ERT-based sensors can achieve TPD distances ranging from 35 mm to 55 mm at the skin's edge and center respectively [39]. For modular design for tactile skin, when multiple receptors are combined for tactile information detection on a larger surface area, there are certain distances between each receptor and different spacings between taxels. In the case of ROBOSKIN, we consider the distance between taxels as the TPD distance, and the result falls within the range of 1 mm to 10 mm [29]. Our proposed tactile sensor exhibits a maximum vertical TPD distance of 5 mm and a horizontal TPD distance of 3 mm, close to that of human fingers. Large area tactile sensors exhibiting a low TPD distance can benefit applications in the human-machine interaction domain, allowing machines to more accurately and precisely perceive and comprehend human tactile inputs across extensive surfaces. Moreover, in virtual reality and augmented reality contexts, such sensors can provide more authentic and precise tactile feedback, thereby enhancing user experience.

Electronic tactile sensing systems demonstrate high sampling rates ranging from 25 Hz to 12.5 kHz [20], [29], [33], [42]. In contrast, our sensor's sampling rate, similar to other vision-based sensors, is limited by the camera's frame rate. However, Luu et al. have successfully used a high-speed camera at 120 Hz to significantly reduce the substantial sampling rate gap between vision-based tactile sensors and electronic-based tactile sensors [38]. The actual sensor response time is dependent on the viscoelastic properties of the material as well as electronic timescales such as charging and discharging times in the case of a capacitive sensor. In modular pressure sensors based on capacitive sensing, algorithms to compensate for thermal drift and viscoelastic relaxation in the sensor were proposed [29]. With good electronics design, electronic timescales are expected to be significantly low, and sensor response times may be dominated by the mechanical viscoelastic behavior. As silicones are predominantly used in both electronic and vision-based sensors, we expect these mechanical timescales to be of a similar range.

Vision systems are commonly employed in robot control and the tactile sensor module based on the piezoluminescent skin interfaces using a single USB and is easy to integrate into existing software for robot control. The demonstration of robot guidance through physical interaction with the tactile sensor showcases its potential to improve intuitive physical human-robot collaboration. The sensor currently optimized for high sensitivity in the low pressure range enables maneuvering the robot with a light touch. The large area tactile sensor showcases a well-rounded performance in terms of spatial resolution, taxel density, localization accuracy with a good pressure estimation accuracy. By further customizing parameters such as sensor geometry, lens configuration, and skin properties, other performance capabilities can be optimized, such as expanded pressure measurement range, higher spatial resolution, or a larger tactile sensing area.

B. Limitations

Due to the utilization of a 30 FPS camera, the response time for tactile event detection is approximately 33 ms. For applications demanding faster response time, a camera with a higher FPS mode to achieve a faster image sampling frequency

needs to be utilized. We set the minimum detectable pressure as 6 kPa to avoid false positives for contact detection due to the presence of image noise in low-light conditions. With advanced signal processing techniques and higher-quality image sensors designed for low-light environments, the minimum detectable pressure could be further reduced. We set the maximum detectable pressure threshold as 20 kPa as the skin remains in a highly sensitive range at this pressure while at the same time ensuring that the acrylic cylinder does not undergo significant deformation, which could compromise pressure estimation accuracy. Additionally, since we used a commercially available low-cost acrylic cylinder, the pressure detection range could be further increased by using higher-strength transparent cylindrical materials that maintain the cylinder's shape under higher pressure. This would help keep the relative positions of the taxels and camera fixed, ensuring accurate measurements and potentially expanding the pressure detection range. The use of 3D-printed PLA material for making the molds also introduces poor tolerances resulting in uneven thickness in the layers of the piezoluminescent skin produced by the casting mold. Employing metal molds can offer more uniformly layered skin structure enhancing the precision and accuracy of pressure estimation.

While the sensor performs well in localizing singular point contacts, its primary application is to localize and provide pressure estimation for distributed normal contacts in which the contact region with an object covers at least a single taxel completely. Additionally, the pressure estimates at the boundaries of contact regions may be inaccurate due to the non-uniform pressure distribution on the boundary taxels. Although not yet realized, marker detection methods using multiple cameras in large area tactile sensors offer the possibility to detect and measure shear forces. However, our method based on the piezoluminescent skin does not offer features for shear force sensing and is restricted to normal force sensing.

IX. Conclusion

In this paper, we introduced a piezoluminescent skin based on a flexible EL panel and a deformable multilayered elastomer structure whose emitted light intensity at a region is dependent on the pressure applied to it. By monitoring the variations in light intensity emitted by the skin using a camera, we achieve contact localization and estimation of pressure magnitude. This methodology provides us with a high spatial resolution, yielding a localization estimation RMSE of 1.92 mm. Furthermore, we achieve a TPD distance of 3 mm to 5 mm, approaching the performance observed in the human fingertip. We demonstrated the guidance of a robot through physical interaction with the tactile sensor mounted as the end-effector showcasing its potential for application to intuitive human-robot collaboration.

In future works, our focus will be directed toward image processing techniques for reducing noise in camera image signals, thus further reducing the minimum measurable pressure and broadening the range of detectable pressures. Additionally, we will work on enhancing the manufacturing processes for multi-layer structured skin to achieve uniformity and augment the precision of pressure estimation. Simultaneously, we will explore the application of this tactile sensing system to augment a robotic arm, facilitating improved human-machine interaction between the robot arm and the operator.

Acknowledgments

We would like to express our sincere gratitude to Huayang Wu for his invaluable support in setting up the demo for robot guidance based on physical interaction with the tactile sensing module. We also thank the reviewers for their helpful suggestions and insightful comments, which have helped improve this manuscript.

References

[1] D. Deflorio, M. Di Luca, and A. M. Wing, "Skin and Mechanoreceptor Contribution to Tactile Input for Perception: A Review of Simulation Models," *Frontiers in Human Neuroscience*, vol. 16, p. 862344, Jun. 2022. [Online]. Available: https://www.frontiersin.org/articles/10.3389/fnhum.2022.862344/full

[2] S.-P. Kim, C. Wallraven, and V. Duchaine, "Editorial: Tactile Intelligence in Robots," *Frontiers in Neurorobotics*, vol. 14, p. 56, Sep. 2020. [Online]. Available: https://www.frontiersin.org/article/10.3389/fnbot.2020.00056/full

[3] C. Chi, X. Sun, N. Xue, T. Li, and C. Liu, "Recent Progress in Technologies for Tactile Sensors," *Sensors*, vol. 18, no. 4, p. 948, Mar. 2018. [Online]. Available: http://www.mdpi.com/1424-8220/18/4/948

[4] W. Mandil, V. Rajendran, K. Nazari, and A. Ghalamzan-Esfahani, "Tactile-Sensing Technologies: Trends, Challenges and Outlook in Agri-Food Manipulation," *Sensors*, vol. 23, no. 17, p. 7362, Aug. 2023. [Online]. Available: https://www.mdpi.com/1424-8220/23/17/7362

[5] S. Horstmann, C. J. Henderson, E. A. Hall, and R. Daly, "Capacitive touchscreen sensing - A measure of electrolyte conductivity," *Sensors and Actuators B: Chemical*, vol. 345, p. 130318, Oct. 2021. [Online]. Available: https://linkinghub.elsevier.com/retrieve/pii/S0925400521008868

[6] H. Nam, K.-H. Seol, J. Lee, H. Cho, and S. W. Jung, "Review of Capacitive Touchscreen Technologies: Overview, Research Trends, and Machine Learning Approaches," *Sensors*, vol. 21, no. 14, p. 4776, Jul. 2021. [Online]. Available: https://www.mdpi.com/1424-8220/21/14/4776

[7] S. Zhang, Z. Chen, Y. Gao, W. Wan, J. Shan, H. Xue, F. Sun, Y. Yang, and B. Fang, "Hardware Technology of Vision-Based Tactile Sensor: A Review," *IEEE Sensors Journal*, vol. 22, no. 22, pp. 21 410–21 427, Nov. 2022. [Online]. Available: https://ieeexplore.ieee.org/document/9911183/

[8] W. Xu, G. Zhou, Y. Zhou, and W. Wu, "A Vision-Based Tactile Sensing System for Multimodal Contact Information Perception via Neural Network," *arXiv:2310.01986*, Oct. 2023. [Online]. Available: https://arxiv.org/abs/2310.01986

[9] R. Li, R. Platt, W. Yuan, A. Ten Pas, N. Roscup, M. A. Srinivasan, and E. Adelson, "Localization and manipulation of small parts using GelSight tactile sensing," in *2014 IEEE/RSJ International Conference on Intelligent Robots and Systems*. Chicago, IL, USA: IEEE, Sep. 2014, pp. 3988–3993. [Online]. Available: http://ieeexplore.ieee.org/document/6943123/

[10] U. H. Shah, R. Muthusamy, D. Gan, Y. Zweiri, and L. Seneviratne, "On the Design and Development of Vision-based Tactile Sensors," *Journal of Intelligent & Robotic Systems*, vol. 102, no. 4, p. 82, Aug. 2021. [Online]. Available: https://link.springer.com/10.1007/s10846-021-01431-0

[11] Y. Zhu, J. Hao, W. Li, J. Yang, and E. Dong, "A new robotic tactile sensor with bio-mimetic structural colour inspired by Morpho butterflies," *Bioinspiration & Biomimetics*, vol. 14, no. 5, p. 056010, Aug. 2019, publisher: IOP Publishing. [Online]. Available: https://dx.doi.org/10.1088/1748-3190/ab3014

[12] W. Yuan, S. Dong, and E. H. Adelson, "GelSight: High-Resolution Robot Tactile Sensors for Estimating Geometry and Force," *Sensors*, vol. 17, no. 12, p. 2762, Dec. 2017, wOS:000423285800062.

[13] S. Dong, W. Yuan, and E. H. Adelson, "Improved GelSight tactile sensor for measuring geometry and slip," in *2017 IEEE/RSJ International Conference on Intelligent Robots and Systems (IROS)*. Vancouver, BC: IEEE, Sep. 2017, pp. 137–144. [Online]. Available: http://ieeexplore.ieee.org/document/8202149/

[14] L. Van Duong and V. A. Ho, "Large-Scale Vision-Based Tactile Sensing for Robot Links: Design, Modeling, and Evaluation," *IEEE Transactions on Robotics*, vol. 37, no. 2, pp. 390–403, Apr. 2021. [Online]. Available: https://ieeexplore.ieee.org/document/9247533/

[15] G. Cao, J. Jiang, C. Lu, D. F. Gomes, and S. Luo, "TouchRoller: A Rolling Optical Tactile Sensor for Rapid Assessment of Textures for Large Surface Areas," *Sensors*, vol. 23, no. 5, p. 2661, Feb. 2023. [Online]. Available: https://www.mdpi.com/1424-8220/23/5/2661

[16] J. Qu, B. Mao, Z. Li, Y. Xu, K. Zhou, X. Cao, Q. Fan, M. Xu, B. Liang, H. Liu, X. Wang, and X. Wang, "Recent Progress in Advanced Tactile Sensing Technologies for Soft Grippers," *Advanced Functional Materials*, vol. 33, no. 41, p. 2306249, Oct. 2023. [Online]. Available: https://onlinelibrary.wiley.com/doi/10.1002/adfm.202306249

[17] P. S. Girão, P. M. P. Ramos, O. Postolache, and J. Miguel Dias Pereira, "Tactile sensors for robotic applications," *Measurement*, vol. 46, no. 3, pp. 1257–1271, Apr. 2013. [Online]. Available: https://linkinghub.elsevier.com/retrieve/pii/S0263224112004368

[18] P. Maiolino, A. Ascia, M. Maggiali, L. Natale, G. Cannata, and G. Mett, "Large Scale Capacitive Skin for Robots," in *Smart Actuation and Sensing Systems - Recent Advances and Future Challenges*, G. Berselli, Ed. InTech, Oct. 2012. [Online]. Available: http://www.intechopen.com/books/smart-actuation-and-sensing-systems-recent-advances-and-future-challenges/large-scale-capacitive-skin-for-robots

[19] L. J. Wood, A. Zaraki, B. Robins, and K. Dautenhahn, "Developing Kaspar: A Humanoid Robot for Children with Autism," *International Journal of Social Robotics*, vol. 13, no. 3, pp. 491–508, Jun. 2021. [Online]. Available: https://link.springer.com/10.1007/s12369-019-00563-6

[20] K. Park, H. Park, H. Lee, S. Park, and J. Kim, "An ERT-based Robotic Skin with Sparsely Distributed Electrodes: Structure, Fabrication, and DNN-based Signal Processing," in *2020 IEEE International Conference on Robotics and Automation (ICRA)*. Paris, France: IEEE, May 2020, pp. 1617–1624. [Online]. Available: https://ieeexplore.ieee.org/document/9197361/

[21] M. K. Johnson and E. H. Adelson, "Retrographic sensing for the measurement of surface texture and shape," in *2009 IEEE Conference on Computer Vision and Pattern Recognition*. Miami, FL: IEEE, Jun. 2009, pp. 1070–1077. [Online]. Available: https://ieeexplore.ieee.org/document/5206534/

[22] W. Yuan, R. Li, M. A. Srinivasan, and E. H. Adelson, "Measurement of shear and slip with a GelSight tactile sensor," in *2015 IEEE International Conference on Robotics and Automation (ICRA)*. Seattle, WA, USA: IEEE, May 2015, pp. 304–311. [Online]. Available: http://ieeexplore.ieee.org/document/7139016/

[23] C. Lin, Z. Lin, S. Wang, and H. Xu, "DTact: A Vision-Based Tactile Sensor that Measures High-Resolution 3D Geometry Directly from Darkness," in *2023 IEEE International Conference on Robotics and Automation (ICRA)*. London, United Kingdom: IEEE, May 2023, pp. 10 359–10 366. [Online]. Available: https://ieeexplore.ieee.org/document/10160796/

[24] W. Li, J. Konstantinova, Y. Noh, Z. Ma, A. Alomainy, and K. Althoefer, "An Elastomer-based Flexible Optical Force and Tactile Sensor," in *2019 2nd IEEE International Conference on Soft Robotics (RoboSoft)*. Seoul, Korea (South): IEEE, Apr. 2019, pp. 361–366. [Online]. Available: https://ieeexplore.ieee.org/document/8722793/

[25] B. Ward-Cherrier, N. Pestell, L. Cramphorn, B. Winstone, M. E. Giannaccini, J. Rossiter, and N. F. Lepora, "The TacTip Family: Soft Optical Tactile Sensors with 3D-Printed Biomimetic Morphologies," *Soft Robotics*, vol. 5, no. 2, pp. 216–227, Apr. 2018, wOS:000419305800001.

[26] Y. Zhang, G. Zhang, Y. Du, and M. Y. Wang, "VTacArm. A Vision-based Tactile Sensing Augmented Robotic Arm with Application to Human-robot Interaction," in *2020 IEEE 16th International Conference on Automation Science and Engineering (CASE)*. Hong Kong, Hong Kong: IEEE, Aug. 2020, pp. 35–42. [Online]. Available: https://ieeexplore.ieee.org/document/9217019/

[27] B. Winstone, C. Melhuish, T. Pipe, M. Callaway, and S. Dogramadzi, "Toward Bio-Inspired Tactile Sensing Capsule Endoscopy for Detection of Submucosal Tumors," *IEEE Sensors Journal*, vol. 17, no. 3, pp. 848–857, Feb. 2017. [Online]. Available: http://ieeexplore.ieee.org/document/7740927/

[28] L. Fu, D. K. Saha, S. Shere, Y. Li, and H. Godaba, "ELTac: A Vision-Based Electroluminescent Tactile Sensing Skin for Force Localization and Magnitude Estimation," *IEEE Sensors Journal*, vol. 24, no. 5, pp. 6846–6855, Mar. 2024. [Online]. Available: https://ieeexplore.ieee.org/document/10413302/

[29] A. Schmitz, P. Maiolino, M. Maggiali, L. Natale, G. Cannata, and G. Metta, "Methods and Technologies for the Implementation of Large-Scale Robot Tactile Sensors," *IEEE Transactions on Robotics*, vol. 27, no. 3, pp. 389–400, Jun. 2011. [Online]. Available: http://ieeexplore.ieee.org/document/5771603/

[30] W. W. Lee, Y. J. Tan, H. Yao, S. Li, H. H. See, M. Hon, K. A. Ng, B. Xiong, J. S. Ho, and B. C. K. Tee, "A neuro-inspired artificial peripheral nervous system for scalable electronic skins," *Science Robotics*, vol. 4, no. 32, p. eaax2198, Jul. 2019. [Online]. Available: https://www.science.org/doi/10.1126/scirobotics.aax2198

[31] A. Nagakubo, H. Alirezaei, and Y. Kuniyoshi, "A deformable and deformation sensitive tactile distribution sensor," in *2007 IEEE International Conference on Robotics and Biomimetics (ROBIO)*. Sanya, China: IEEE, Dec. 2007, pp. 1301–1308. [Online]. Available: http://ieeexplore.ieee.org/document/4522352/

[32] Y. Kato, T. Mukai, T. Hayakawa, and T. Shibata, "Tactile Sensor without Wire and Sensing Element in the Tactile Region Based on EIT Method," in *2007 IEEE Sensors*. Atlanta, GA, USA: IEEE, 2007, pp. 792–795. [Online]. Available: http://ieeexplore.ieee.org/document/4388519/

[33] K. Park, H. Lee, K. Kuchenbecker, and J. Kim, "Adaptive Optimal Measurement Algorithm for ERT-Based Large-Area Tactile Sensors," *IEEE/ASME Transactions on Mechatronics*, vol. 27, no. 1, pp. 304–314, Feb. 2022. [Online]. Available: https://ieeexplore.ieee.org/document/9369139/

[34] R. Dahiya, N. Yogeswaran, F. Liu, L. Manjakkal, E. Burdet, V. Hayward, and H. Jorntell, "Large-Area Soft e-Skin: The Challenges Beyond Sensor Designs," *Proceedings of the IEEE*, vol. 107, no. 10, pp. 2016–2033, Oct. 2019. [Online]. Available: https://ieeexplore.ieee.org/document/8858052/

[35] M. Lowther, A. Tzemanaki, and H. Hauser, "Design and Characterisation of Salt-E-Skin: Soft Saline-Filled Large-Scale Tactile E-Skin," in *2024 IEEE 7th International Conference on Soft Robotics (RoboSoft)*. San Diego, CA, USA: IEEE, Apr. 2024, pp. 734–739. [Online]. Available: https://ieeexplore.ieee.org/document/10521940/

[36] Zhengyou Zhang, "Flexible camera calibration by viewing a plane from unknown orientations," in *Proceedings of the Seventh IEEE International Conference on Computer Vision*. Kerkyra, Greece: IEEE, 1999, pp. 666–673 vol.1. [Online]. Available: http://ieeexplore.ieee.org/document/791289/

[37] H. Yao, W. Yang, W. Cheng, Y. J. Tan, H. H. See, S. Li, H. P. A. Ali, B. Z. H. Lim, Z. Liu, and B. C. K. Tee, "Near–hysteresis-free soft tactile electronic skins for wearables and reliable machine learning," *Proceedings of the National Academy of Sciences*, vol. 117, no. 41, pp. 25 352–25 359, Oct. 2020. [Online]. Available: https://pnas.org/doi/full/10.1073/pnas.2010989117

[38] Q. K. Luu, N. H. Nguyen, and V. A. Ho, "Simulation, Learning, and Application of Vision-Based Tactile Sensing at Large Scale," *IEEE Transactions on Robotics*, vol. 39, no. 3, pp. 2003–2019, Jun. 2023. [Online]. Available: https://ieeexplore.ieee.org/document/10054516/

[39] H. Lee, K. Park, J. Kim, and K. J. Kuchenbecker, "Piezoresistive textile layer and distributed electrode structure for soft whole-body tactile skin," *Smart Materials and Structures*, vol. 30, no. 8, p. 085036, Aug. 2021. [Online]. Available: https://iopscience.iop.org/article/10.1088/1361-665X/ac0c2e

[40] H. Lee, K. Park, J. Kim, and K. J. Kuchenbecker, "Internal Array Electrodes Improve the Spatial Resolution of Soft Tactile Sensors Based on Electrical Resistance Tomography," in *2019 International Conference on Robotics and Automation (ICRA)*. Montreal, QC, Canada: IEEE, May 2019, pp. 5411–5417. [Online]. Available: https://ieeexplore.ieee.org/document/8794276/

[41] H. Lee, H. Park, G. Serhat, H. Sun, and K. J. Kuchenbecker, "Calibrating a Soft ERT-Based Tactile Sensor with a Multiphysics Model and Sim-to-real Transfer Learning," in *2020 IEEE International Conference on Robotics and Automation (ICRA)*. Paris, France: IEEE, May 2020, pp. 1632–1638. [Online]. Available: https://ieeexplore.ieee.org/document/9196732/

[42] K. Park and J. Kim, "Neural-Gas Network-Based Optimal Design Method for ERT-Based Whole-Body Robotic Skin," *IEEE Transactions on Robotics*, vol. 38, no. 6, pp. 3463–3478, Dec. 2022. [Online]. Available: https://ieeexplore.ieee.org/document/9823397/

[43] H. Lee, H. Sun, H. Park, G. Serhat, B. Javot, G. Martius, and K. J. Kuchenbecker, "Predicting the Force Map of an ERT-Based Tactile Sensor Using Simulation and Deep Networks," *IEEE Transactions on Automation Science and Engineering*, vol. 20, no. 1, pp. 425–439, Jan. 2023. [Online]. Available: https://ieeexplore.ieee.org/document/9737320/

[44] P. Mittendorfer and G. Cheng, "Humanoid Multimodal Tactile-Sensing Modules," *IEEE Transactions on Robotics*, vol. 27, no. 3, pp. 401–410, Jun. 2011. [Online]. Available: http://ieeexplore.ieee.org/document/5711674/

[45] A. Stilli, L. Grattarola, H. Feldmann, H. A. Wurdemann, and K. Althoefer, "Variable Stiffness Link (VSL): Toward inherently safe robotic manipulators," in *2017 IEEE International Conference on Robotics and Automation (ICRA)*. Singapore, Singapore: IEEE, May 2017, pp. 4971–4976. [Online]. Available: http://ieeexplore.ieee.org/document/7989578/

[46] J. M. Gandarias, Y. Wang, A. Stilli, A. J. Garcia-Cerezo, J. M. Gomez-de Gabriel, and H. A. Wurdemann, "Open-Loop Position Control in Collaborative, Modular Variable-Stiffness-Link (VSL) Robots," *IEEE Robotics and Automation Letters*, vol. 5, no. 2, pp. 1772–1779, Apr. 2020. [Online]. Available: https://ieeexplore.ieee.org/document/8972614/

[47] Q. K. Luu, D. Q. Nguyen, N. H. Nguyen, and V. A. Ho, "Soft Robotic Link with Controllable Transparency for Vision-based Tactile and Proximity Sensing," in *2023 IEEE International Conference on Soft Robotics (RoboSoft)*. Singapore, Singapore: IEEE, Apr. 2023, pp. 1–6. [Online]. Available: https://ieeexplore.ieee.org/document/10122059/

[48] K. U. Maheswari, R. G. Devi, and A. J. Priya, "Estimation of Tactile Sensation by Two Point Discrimination among 18 Years Old People," *Journal of Pharmaceutical Research International*, pp. 355–363, Nov. 2021. [Online]. Available: https://journaljpri.com/index.php/JPRI/article/view/3936

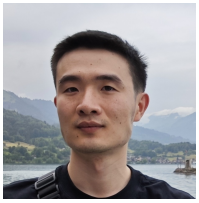

Ruxiang Jiang received the B.Eng. degree in Electrical Engineering and Automation from Wenzhou Business College, Wenzhou, Zhejiang, China, in 2020, and the M.Sc. degree in Robotics and Autonomous Systems from the University of Sussex, Brighton, U.K., in 2022, where he is currently pursuing a Ph.D. degree in engineering with the University of Sussex, Brighton, U.K. His research interests include image processing, tactile sensing, and machine vision.

Lanhui Fu received the B.S. degree from Zhengzhou University, Zhengzhou, China, in 2009, the M.S. degree from the Harbin Institute of Technology, Harbin, China, in 2012, and the Ph.D. degree from South China Agricultural University, Guangzhou, China, in 2022. She is currently a Lecturer at the School of Electronics and Information Engineering, Wuyi University, Guangdong, China. Her research interests include image processing, tactile sensing, machine vision, and deep learning.

Yanan Li (Senior Member, IEEE) received a Ph.D. degree in Robotics from the National University of Singapore, in 2013, and B.Eng. and M.Eng. degrees in Automation from the Harbin Institute of Technology, China, in 2006 and 2008, respectively. He is currently a Reader in Robotics and Director of the Centre for Robotics and Sensing Technologies (CROSS-Tech), Department of Engineering and Design, University of Sussex, U.K. From 2015 to 2017, he was a Research Associate with the Department of Bioengineering, Imperial College London, U.K. From 2013 to 2015, he was a Research Scientist with the Institute for Infocomm Research, Agency for Science, Technology and Research, Singapore. His general research interests include human-robot interaction, robot control, and control theory and applications.

Hareesh Godaba received the B.Tech. (Hons.) degree in mechanical engineering from the Indian Institute of Technology (IIT) Bhubaneswar, Bhubaneswar, India, in 2013, and the Ph.D. degree in mechanical engineering from the National University of Singapore (NUS), Singapore, in 2018. He is currently a Lecturer in the Department of Mechanical Engineering at the University of Southampton, Southampton, U.K. He was a Research Associate at the Queen Mary University of London from 2018 to 2020 and a Lecturer at the University of Sussex from 2020 to 2024. His research interests include soft robotics, electroactive technologies, and tactile sensing.